
Article:
Sosa Gallardo, A.F. and Provis, J.L. (2022) Early-age characterisation of Portland cement by impedance spectroscopy. Advances in Cement Research, 34 (12). pp. 542-559. ISSN 0951-7197

https://doi.org/10.1680/jadcr.21.00103

Early-age characterisation of Portland cement by impedance spectroscopy

Aldo F. Sosa Gallardo, John L. Provis

Department of Materials Science and Engineering, The University of Sheffield, Sir Robert Hadfield building, S1 3JD, United Kingdom.

*corresponding author: j.provis@sheffield.ac.uk, phone number: +44 114 222 5490.

Abstract

This paper applies alternating current impedance spectroscopy to assess the effect of different sand, anhydrite, and water contents on the electrochemical response of Portland cement in the early stages of hydration. Potential factors that may affect impedance measurements and data interpretation are also discussed, such as the complexity of cement chemical composition, its physical properties and hydration kinetics, and technique limitations. The impedance data obtained are benchmarked against different supporting techniques and literature data, showing a strong relationship among hydration rates as determined by thermochemistry, setting time measurements by physical approaches, pore fluid chemistry, electrical conductivity, and the impedance behaviour observed. The results demonstrate that ACIS is a sensitive technique to assess cement hydration, enabling differentiation of changes in the water and cement content, hydration degree, and microstructural development during the first 24 hours after mixing.

Keywords: Cement hydration, Alternating current impedance spectroscopy, Thermochemistry, Setting time, Pore solution.

1. Introduction

To understand the influence of different cement mix design parameters on the kinetics of reaction, microstructural and pore solution development during cement hydration, assessment with different analytical tools and techniques is needed. There are many well-

established tools used in this field worldwide, yet a holistic characterisation of cement reactions from the fresh to the hardened state remains elusive. Techniques such as calorimetry and rheometry are effective in the first stages of the reaction process but cannot provide detailed information as the microstructure evolves after setting, whereas techniques such as microscopy and diffractometry are very difficult to apply before the time of setting. The fundamental aim of this paper is to demonstrate that impedance spectroscopy is a technique with the potential to fill this very significant need in the cements characterisation community.

The hydration of cement starts immediately when cement powder is mixed with water, triggering different (simultaneous and consecutive) chemical reactions that lead to the dissolution of clinker phases; nucleation, precipitation and crystallization of different hydration products; release of heat; consumption of water; and densification of the hardened cement hydrate microstructure (Mehta and Monteiro, 2006; Hewlett and Liska, 2019). For over 100 years, understanding the complexity of cement hydration at early ages and the influence of admixtures on the final properties, kinetic mechanism(s) and microstructural development of cements has been a growing interest in industry and academia (Langan *et al.*, 2002; Lothenbach *et al.*; Cruz *et al.*, 2013; Tang *et al.*, 2017).

Numerous methods and techniques have been used to assess cement hydration. One of these techniques is isothermal calorimetry (IC), a high precision and accurate technique that measures the heat produced by the hydration of Portland cement. IC can assess hydration stages, release of heat (timing, heat evolution profile), and the influences of mix design parameters and particle size distribution. However, the information obtained via this technique during the initial “dormant” period and the long-term hydration period is limited (Haines, 2002; Höhne *et al.*, 2003; Gerstig and Wadsö, 2010). Another method is the Vicat needle test which assesses the initial and final setting times of cementitious materials. This test is based on physical changes in the cement paste leading to increased yield stress (and eventually the generation of strength by

solidification) (Romano *et al.*, 2018) but this is essentially a two-point measurement determining initial and final setting times.

The assessment of the development of pore fluid chemistry during hydration supports and complements the understanding of the kinetics and mechanism(s) of hydration, electrical behaviour, the interactions between solid and aqueous phases. Techniques such as ion chromatography and inductively coupled plasma optical emission spectroscopy are used in cement research to assess the ionic species (e.g. Ca^{2+}, K^{+}, Na^{+}, SO_4^{2-} and OH^{-}) in the liquid solution of cement paste (Brouwers and Van Eijk, 2003; Lothenbach *et al.*, 2007; Caruso *et al.*, 2017). However, a complete qualitative analysis of the pore solution is difficult to obtain due to the rate of reactions which necessitate labour-intensive regular sampling, and some instrumental limitations in the analysis of highly concentrated alkaline fluids (Dewah *et al.*, 2002; Wong and Buenfeld, 2009; Lura *et al.*, 2012).

Another technique that has been more sporadically used in cement research is alternating current impedance spectroscopy (ACIS), which measures the electrical response of a system as a function of frequency. This technique provides information related to the electrical and chemical behaviour, and to the microstructure of diverse materials, making ACIS potentially a very powerful characterisation technique that is applicable to both solid and liquid states of the cement hydration process. The impedance response obtained at high frequency is considered to represent the material bulk response, and the signal at low frequency is the material-electrode response (Barsoukov and Macdonald, 2005; Orazem and Tribollet, 2008; Yuan *et al.*, 2010). The ACIS assessment of cement hydration is possible by considering the cementitious material as an equivalent circuit whereby the electrical behaviour depends on the resistance and reactance response of the system. However, in the early stages of cement hydration, ACIS measurements show certain limitations (e.g. current dispersion, data interpretation, electrode and parasitic effects) (Hsieh *et al.*, 1996; Mason *et al.*, 1998; Spragg *et al.*,

2013; Hu *et al.*, 2019) which have restricted the more widespread application of this technique to the study of cement hydration after some initially promising early publications in past decades.

ACIS is not yet fully accepted by the cement research community and industry. The need for further technique development has been particularly evident in many cement studies at early hydration ages (≤24 hrs) at which the available ACIS information is very limited due to instrument and data interpretation limitations, the complex chemical composition and continuous evolution of the pore solution, and microstructural development of cement paste. ACIS is a highly sensitive technique, but the measurements obtained can be affected by parasitic effects which are often overlooked, leading to data misinterpretation. As a result of this limitation, ACIS experimentation for in-situ analysis of cementitious materials requires caution during experimentation. Also, ACIS measurements show certain additional limitations at high frequencies during early cement hydration ages, restricting the use of ACIS for studying cement hydration.

Recent work has focused on the development of strategies to minimise the interferences of important parasitic effects in ACIS data at early age, and has opened new opportunities to apply ACIS to gain meaningful data to describe and further understand cement hydration (Xiao and Wei, 2011; Wei *et al.*, 2012; Liao and Wei, 2014).

The objective of this paper is to assess the early hydration process of Portland cements at different sand, anhydrite, and water contents by evaluating the electrochemical (ACIS), thermochemical (IC), and setting time (Vicat) responses, and by comparison with pore solution compositional data available in the literature. Comparison among these techniques is important to understand the major aspects that influence the

electrochemical behaviour of cement pastes during the first 24 hrs after mixing, both before and after setting.

2. Materials and methods

2.1 Sample preparation

Samples were prepared at room temperature (20 ± 3 °C and 50 ± 15% relative humidity) by mixing water with grey Portland cement (Cemex; gPc) or white Portland cement (wPc; Lafarge Blue Circle Snowcrete) both classified as CEM I 52.5R under BS EN 197-1, at different water to cement ratios (w/c); or different replacement levels of standard silica sand under EN 196-1; or anhydrite (A; Fisher C/2440/60, >95%). The chemical compositions and physical properties of the two cements are given in Table 1, and the specific mixes tested are outlined in section 3.

Each sample was hand mixed by combining the components for 3 min to form a homogeneous paste, and then transferred into analysis vessels: 300 g into a custom-designed cell as described below (for ACIS measurements), or 20 g into a high density polyethylene ampule (for thermochemistry measurement), or 300 g into a plastic mould (for the Vicat setting test). Prior to the start of the analysis, all samples were vibrated for 2 min to reduce the level of entrapped air bubbles (Sosa Gallardo and Provis, 2020).

Table 1. Chemical composition of wPc and gPc as determined by X-ray fluorescence analysis, and average particle size d_{50} from laser particle sizing (Sosa Gallardo and Provis, 2020).

Compound (wt.%)	**wPc**	**gPc**
SiO_2	23.7	19.8

Al_2O_3	3.9	4.9
CaO	66.5	62.5
Fe_2O_3	0.2	3.1
MgO	0.9	1.6
Na_2O	0.2	0.4
K_2O	0.5	0.9
SO_3	2.6	3.7
TiO_2	-	0.2
Others	1.0	-
*LOI	1.2	2.4
d_{50} (μm)	11.0	13.0

*LOI: Loss on ignition at 950°C

To characterise the microstructure of the cement samples by SEM at early hydration ages, the hydration of cement was stopped by a solvent exchange method:

- At 4 hrs after mixing, 1 g of hydrating paste was taken out from the plastic vial and filtered using filter papers. Then isopropanol was added, stirring constantly. The powder obtained was then dried in a desiccator for 48 hours.
- At 8, 12, and 24 hrs after mixing, the plastic vials were cut into 2 cm slices with a slow-speed diamond saw. Each slice was immersed three times in a 1:5 sample to solvent volume ratio of isopropanol (Sigma-Aldrich) for 24 hours, then the slices were dried in a desiccator for 48 hours.

After stopping cement hydration, each sliced sample was polished with a 1200 grain size silicon carbide paper until a flat shiny surface was obtained. Each slice was then sectioned to isolate a small piece and cleaned from residual dust. The small piece was then placed into a cylindrical mould to be resin coated with Epoxycure 2 (Buehler, mixing ratio: 4 parts resin to 1 part hardener by volume,) to support the microstructure.

156 Once the resin samples were dried (after 24 hours), the samples were polished
157 successively with 400, 800 and 1200 grain size silicon carbide paper to remove any thin
158 layer of resin and uncover the sample surfaces. The samples were then polished with
159 diamond paste (Met Prep) of different particle sizes (6, 4, 1 and 0.25 μm). After polishing,
160 samples were cleaned for 48 hours in an ultrasonic bath with isopropanol and dried in a
161 desiccator. Polished sample surfaces were then carbon coated to obtain a conductive
162 layer before analysis (Scrivener *et al.*, 2017), and to mount the samples onto SEM
163 specimen holders, conductive carbon tabs were added to the unpolished sample
164 surfaces. Finally, for charging effect purposes silver paint (Agar) was used as a
165 conductive connection to the carbon coated surface, the carbon tab and the sample
166 holder.
167
168 *2.2 Instrumental analysis*
169
170 Samples were subjected to ACIS measurements using an impedance analyser with a
171 single channel (Metrohm AutoLab, PGSTAT204) connected to a custom two-electrode
172 cell design (Fig. 1) (Metrohm Autolab B.V, 2011). The custom cell was designed using a
173 cylindrical polypropylene container (ϕ6 × 11.2 cm), filled to a depth of 7.5 cm for each
174 experiment) and two threaded stainless-steel electrodes (ϕ0.3 × 7 cm). To avoid sample
175 leakage, the electrodes were inserted in the bottom face of the container and attached
176 with a hard-plastic adhesive. The design of the initial cell was based on the characteristics
177 of its constituents, simplicity of the design, low cost of the materials, its performance,
178 reproducibility and convenience for laboratory experimentation (Sosa Gallardo and
179 Provis, 2020). To minimise parasitic effects during the ACIS analysis, the final design of
180 the cell was carried out by optimising, according to their capacity and performance, the
181 experimental setup and the cell components, Table 2.
182
183 Table 2. Basis of the initial cell design (Sosa Gallardo and Provis, 2020).

Two-electrode setup	- Commonly used to measure the potential and bulk resistance across the sample. - Allows the assessment of electrochemical impedance measurements at high frequency (>100 kHz).
Amplitude	- It was observed that the optimal amplitude to avoid nonlinear effects in Portland cement was 10 mV.
Sample dimensions	- Allow measuring the bulk properties of the sample. - Allow using a small perturbation amplitude without affecting the measurement.
Polypropylene container	- Inexpensive. - Inert to the majority of chemical reactions. - Suitable for alkaline solutions. - More volume per unit wall area (cylindrical geometry) .
Leads arrangement	
Length	As it was observed that an increase in the lead length increases the parasitic effects, it was decided to use 150 cm of length. It was not possible to further reduce the length of the leads due to the equipment limitations.
Quality	- Conductor, insulation, binder, braid, jacket, connectors, and alignment of the connection between the leads and the electrodes were tested so that they could be suitable for the experiment
Electrode properties	
Material	- Stainless steel has suitable corrosion resistance properties in high alkaline solutions.
Geometry and dimensions	- High active surface area. - Allow more current density at the surface. - Potential and current distribution is uniform. - Electric field across the sample is uniform. - Increase measurement sensitivity.
Position	- It was selected to introduce the electrodes in the bottom face of the custom cell since this location showed a better performance on the ACIS measurements, without cracks appearing in the hardened cement, and ensuring consistent measurement of the cement paste
Texture	- Improves contact between the electrodes and the cement paste. - Increases the surface-active area of the electrode.
Separation	- Increases the signal-to-noise ratio. - Used to assess mutual and self-inductance.

184

ACIS measurements (50 data points per cycle) were collected at room temperature over a frequency range of 100 Hz to 1 MHz, an applied perturbation amplitude of 10 mV and current range up to 1 mA. The frequency range 1 MHz - 100 Hz, were found to be representative of the most important behaviour in this analysis (i.e. cement bulk response, cement-electrode response). Measurements were triplicated and obtained every 5 min during the first 24 hrs after mixing. The measurements were consistent to within at 8% 5 min, 3% at 24 hrs, and the timing of the main features observed was repeatable to within ± 5 min (Sosa Gallardo and Provis, 2020). The data obtained from this technique are conveniently represented as a Nyquist plot, where the imaginary component is conventionally plotted as -Z'' and the real component is Z' of the complex impedance formalism, Z*.

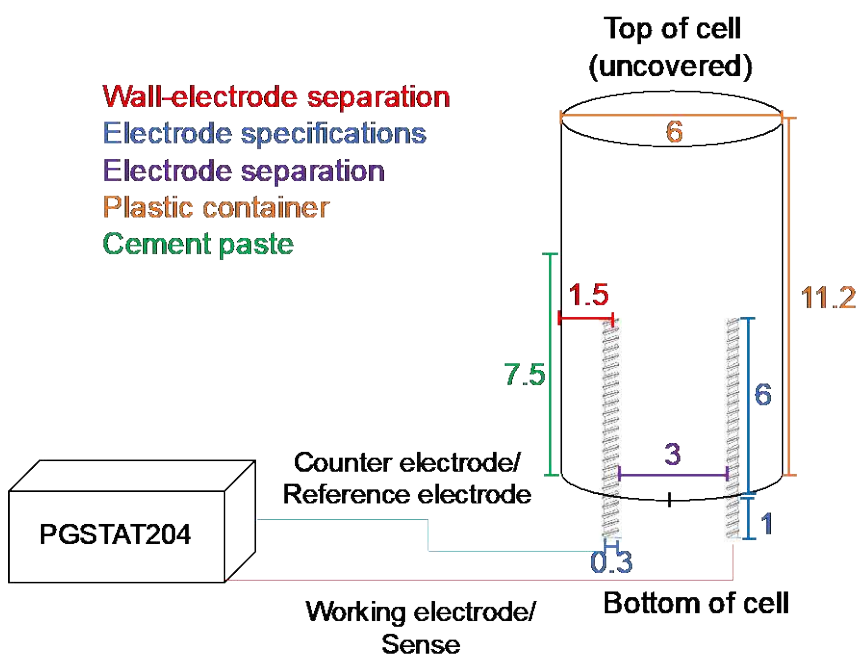

Fig. 1. ACIS custom-cell design diagram (scale in cm) (Sosa Gallardo and Provis, 2020).

SEM characterisation was carried out with a Hitachi TM3030 instrument equipped with an energy dispersive X-ray analyser (EDX) for elemental analysis. The modes used

202 in the analysis were backscattered electron imaging (BSE) and EDX elemental mapping
203 with an accelerating voltage of 15 kV.
204
205 Isothermal calorimetry tests were conducted during the first 24 hrs after mixing
206 according to the ASTM C1679 standard procedures (ASTM International, 2017) using an
207 8-channel TAM Air isothermal calorimeter (TA Instruments). Initial and final setting times,
208 according to EN 196-3, were determined by applying 90 penetrations during the first 15
209 hrs after mixing, using a Vicatronic apparatus (Matest, E044N).
210
211 *2.3 Calibration and ACIS measurements correction procedure*
212
213 The impedance response of the cell in a short circuit arrangement (without sample) was
214 measured before the samples were tested, to enable minimisation of the parasitic effects
215 associated with the cell components and leads. The measurement correction was made
216 at each frequency, considering the ACIS response of the cement sample and the parasitic
217 effects as additional quantities in the final ACIS measurements (Soboleva *et al.*, 2008;
218 Raikova *et al.*, 2009; Sosa Gallardo and Provis, 2020).
219

220 **3. Experimental methodology**

221
222 To support ACIS data interpretation, five groups of Portland cements at different w/c
223 ratios, and replacement levels of sand or anhydrite, were assessed by ACIS
224 measurements and supported by calorimetry and setting tests. The first group consisted
225 of wPc hydrated at different w/c ratios (0.35-0.60). Table 3 shows the sample
226 specifications of each of the other groups, which were all formulated at a constant w/c
227 ratio of 0.45. Grey cement was used as a comparison to the wPc results; three sand
228 replacement levels and three dosages of anhydrite were tested.
229
230

Table 3. Sample specifications.

No.	Parameter	Amount			*w/c
1	**wPc (%)**	100			0.35-0.60
2	**wPc (%)**	100			0.45
3	**gPc (%)**	100			
4	**wPc (%)**	80	60	40	
	Sand (%)	20	40	60	
5	**wPc (%)**	100	99	90	
	Anhydrite (%)	0.5	1	10	

The Nyquist plot format was used to display and analyse ACIS measurements. Inductance effects were identified via ACIS values falling below the real axis. The real and imaginary components of the signal measured at 100 Hz and 1 MHz were plotted as a function of time. This enabled observation of a distinctive perspective of the impedance data obtained, separating the time dependence of the high-frequency and low-frequency responses.

Conductivity measurements were obtained from the resistivity of each cementitious paste by dividing the intercept point on the real axis of the Z* plots into a cell constant, which was obtained by measuring different concentrations of NaOH solutions of known conductivity (National Institute of Standards and Technology, 2004; Provis *et al.*, 2008; Rosemount Analytical, 2010; Heath *et al.*, 2019).

4. Results and discussion

4.1 White Portland cement and grey Portland cement (wPc and gPc)

The presence of significant quantities of Fe_2O_3 and MnO gives gPc, one of the most used cements, its grey colour. On the other hand, wPc which is usually used for aesthetic architectural applications, differs from gPc by having a limited amount of Fe_2O_3, and MnO, higher free CaO content, and a higher content of C_3A. It is sometimes often more finely ground, as is the case for the cements studied here. In general wPc, due to the high energy consumption required for its production, is more expensive than Portland cement. (Taylor, 1997; Mehta and Monteiro, 2006; Hewlett and Liska, 2019). The pore solution of wPc is slightly different from other Portland cements since it has a lower alkali content (i.e. K and Na), producing a decrease in the available content of SO_4^{2-} and OH^- ions available to react with C_3A during hydration, lowering the production of ettringite (Richardson *et al.*, 2016; Sanjuán *et al.*, 2019).

The calorimetric curves of wPc and gPc during the first 24 hrs after mixing are shown in Fig. 2a. The hydration stage timings in wPc and gPc are similar, however a higher release of heat is observed for wPc paste due to the rapid hydration of C_3A, ettringite formation, and the smaller particle size and higher surface area of this cement. At the end of the acceleration period gPc shows two shoulders (between 6 and 8 hrs) which are attributed to the hydration of C_3S and C_3A, and the formation of C-S-H and ettringite (Li and Coleman, 2014; Sáez del Bosque *et al.*, 2015; Richardson *et al.*, 2016).

Fig. 2b shows the penetration depth of the Vicat needle into wPc and gPc. The initial and final setting times are reached at similar times, with setting observed for the gPc paste slightly faster than the wPc. This is attributed to a more stable transformation of ettringite into AFm and the formation of secondary phases as a result of a higher sulphate content in gPc paste, showing an earlier acceleration and more gradual heat release (Ylmén *et al.*, 2009; Sáez del Bosque *et al.*, 2015).

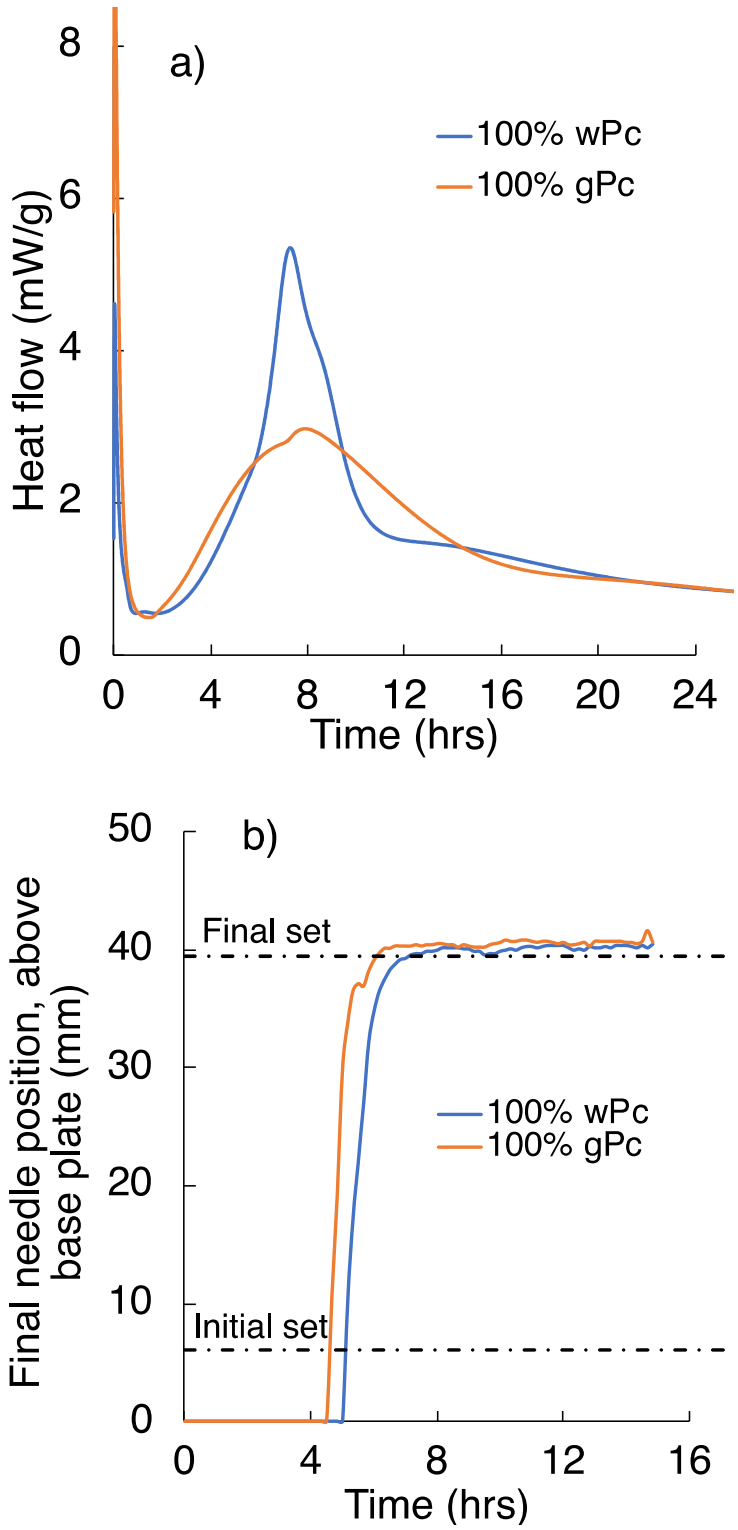

Fig. 2. wPc and gPc hydration at w/c = 0.45: a) heat flow, b) Vicat determination of setting time.

The ACIS and resistivity/conductivity measurements of wPc and gPc during the first 24 hrs after mixing are shown in Fig. 3a-b. Fig. 3c and 3d show the ACIS response of wPc and gPc by representing the measurements in terms of resistance and reactance as a function of time and frequency.

At early ages and in both pastes, a semicircular arc of small impedance is obtained due to the high conductivity of the cement paste (Fig. 3a). At high frequency, wPc shows a higher impedance and resistance than gPc, an effect that is attributed to the higher particle surface area, the particle size distribution, and the conversion of C_3A to ettringite, leading to an early-age paste that contains a higher volume of hydrate products (Zhang and Napier-Munn, 1995). The wPc shows a conductivity perturbation at 1 hr after mixing, and gPc shows the same perturbation at approximately 2 hrs after mixing (Fig. 3b) (Sosa Gallardo and Provis, 2020). Also, the dormant period in Fig. 2a is longer for wPc paste, but the ACIS measurements do not change.

During the acceleration period, the conductivity of the gPc paste drops considerably faster than that of the wPc paste, while the gPc and wPc bulk resistance increase slightly. This drop is attributed to the decrease of ionic concentrations and their reduced mobility as the microstructure evolves (Backe *et al.*, 2001; Brouwers and Van Eijk, 2003). The wPc ACIS measurements are affected by parasitic effects at high frequency at around 4 hrs after mixing, while gPc ACIS measurements are affected at longer times. The appearance of parasitic effects in the impedance measurements was associated with the beginning of this period in which the ionic species concentrations and pH rises, incorporating alkaline species into the clinker and hydrated phases (Sosa Gallardo and Provis, 2020). Also, during this period, the heat release increases as the crystallisation of CH and the precipitation-nucleation of C-S-H take place (Bullard *et al.*, 2011; Cruz *et al.*, 2011; Bligh *et al.*, 2016; Azarsa and Gupta, 2017).

During the deceleration period, both cement pastes show an increasing bulk resistance (Fig. 3c). At this point the capillary aqueous phase and pore connectivity are reduced, the microstructure is more fully developed (with limited available space for new hydrated products), and C-S-H gel keeps increasing (Fig. 4a-b), (Dotelli and Mari, 2001; Ylmén *et al.*, 2010; Pang *et al.*, 2013). At approximately 14 hrs, the high frequency ACIS data for gPc are affected by parasitic effects (Fig. 3c-d), which merits further investigation.

At later ages and at high frequency, where the wPc impedance and bulk resistance values are greater than in gPc pastes (Fig. 3c), there is a decreasing tendency in the conductivity and parasitic effects of both pastes due to the reduction of free water content, and limited space for growth of new hydrated products via constant microstructural development, leading to a larger bulk semicircular arc (Christensen *et al.*, 1994; McCarter, 1994; Dong *et al.*, 2014; Azarsa and Gupta, 2017).

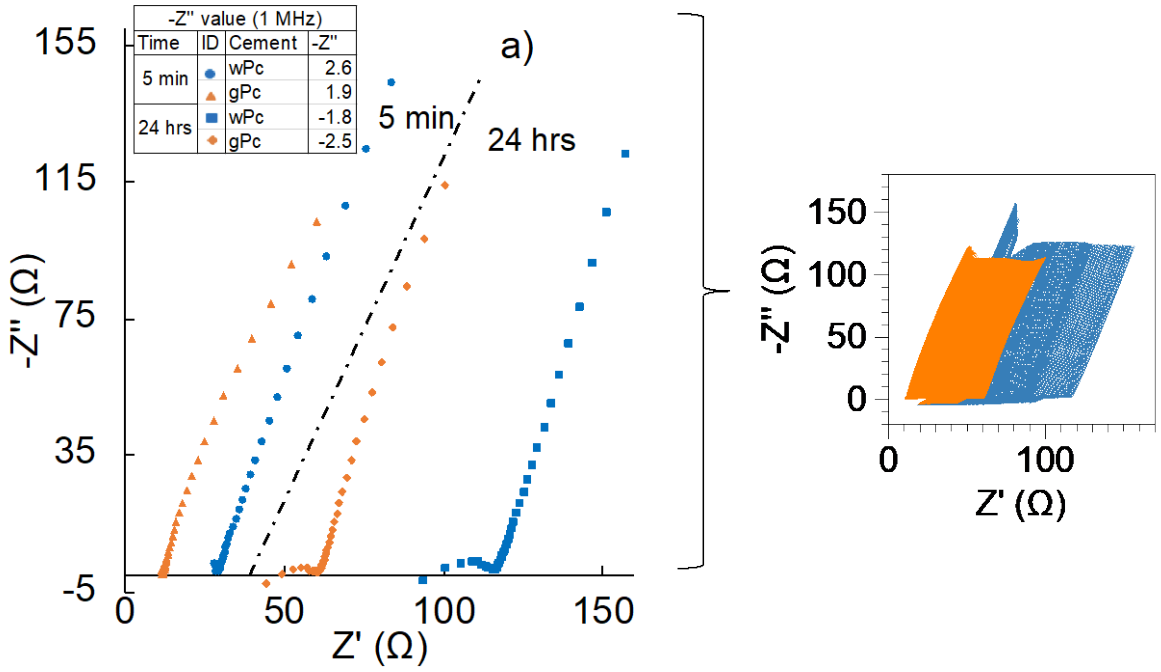
-Z'' value (1 MHz)
Time
ID
Cement
-Z''
5 min
wPc
2.6
gPc
1.9
24 hrs
wPc
-1.8
gPc
-2.5
a)
5 min
24 hrs
155
115
75
35
-5
-Z'' (Ω)
0
50
100
150
Z' (Ω)
150
100
50
0
-Z'' (Ω)
0
100
Z' (Ω)

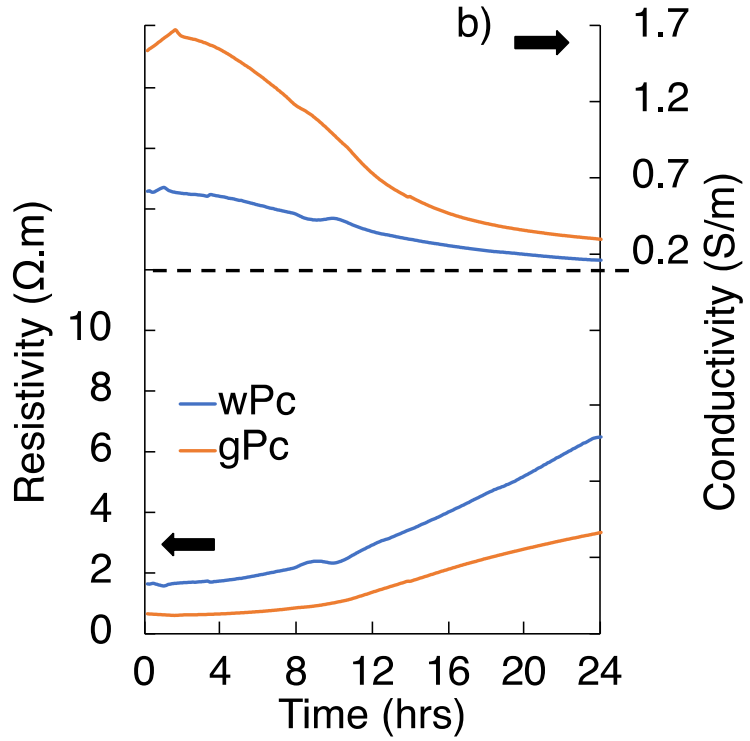
b)
1.7
1.2
0.7
0.2
Conductivity (S/m)
10
8
6
4
2
0
Resistivity (Ω.m)
wPc
gPc
0
4
8
12
16
20
24
Time (hrs)

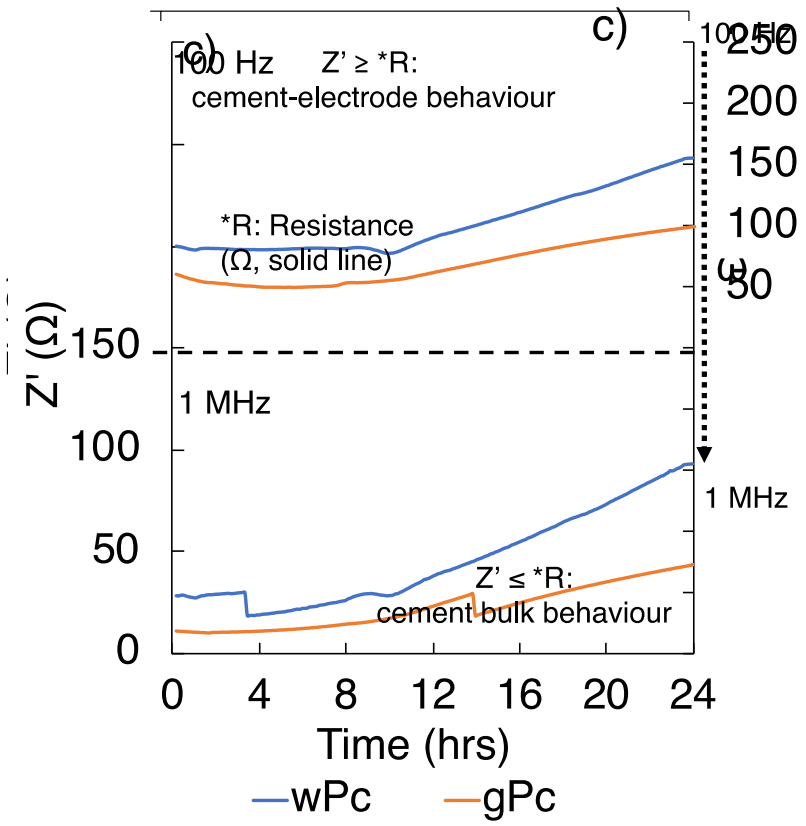
c)
100 Hz
Z' ≥ *R:
cement-electrode behaviour
*R: Resistance
(Ω, solid line)
1 MHz
Z' ≤ *R:
cement bulk behaviour
Z' (Ω)
150
100
50
0
0
4
8
12
16
20
24
Time (hrs)
250
200
150
100
50
1 MHz
wPc
gPc

328

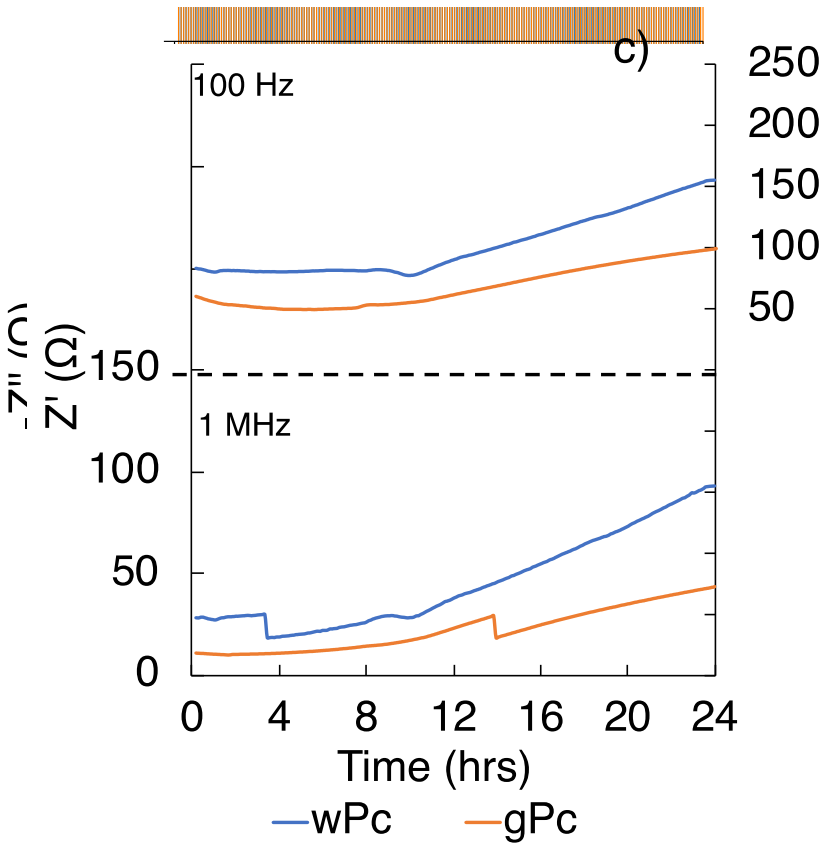

Fig. 3. ACIS response of wPc and gPc pastes at w/c = 0.45 as indicated in the legend: a) Nyquist plots; b) conductivity and resistivity; and from 1 MHz to 100 Hz c) real component and d) imaginary component.

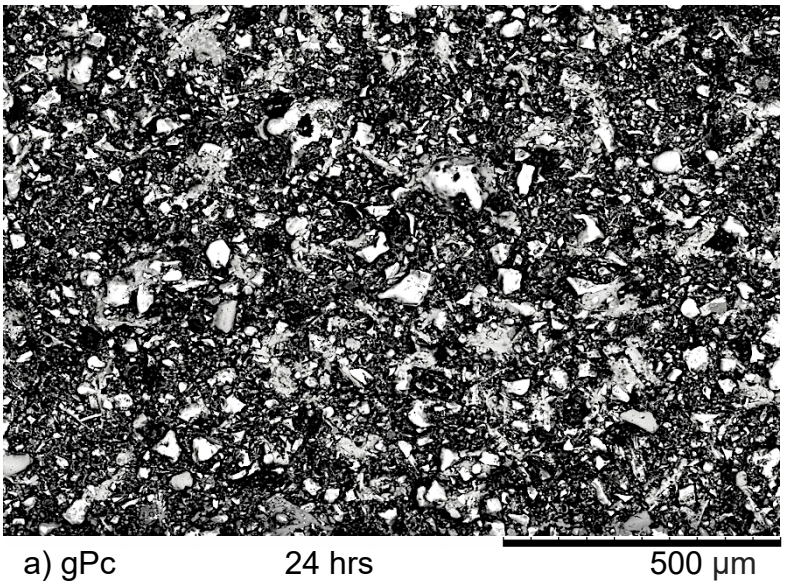

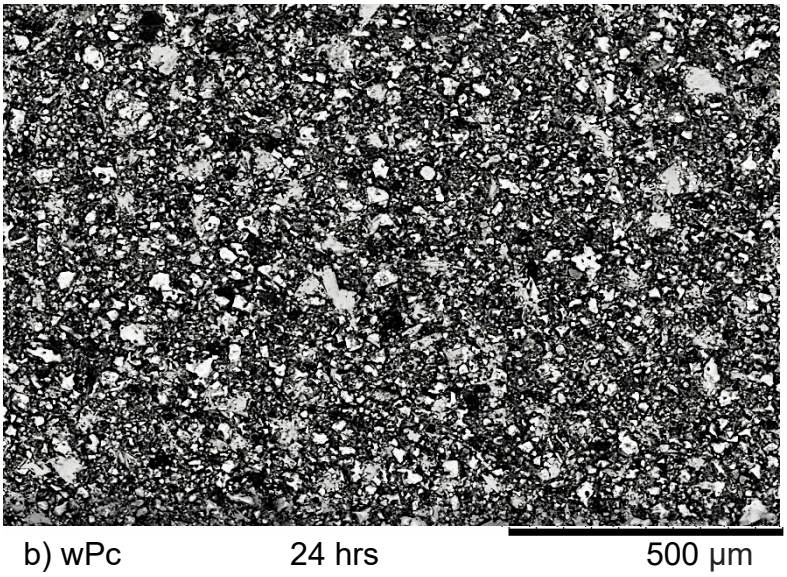

Fig. 4. SEM images of gPc (a) and wPc (b) paste at 24 hrs after mixing.

4.2 Effects of water to cement ratio (w/c)

As the w/c ratio affects the space among the cement particles, kinetics of hydration, setting-hardening times, and microstructure, the water content becomes a major factor influencing the hydration mechanisms and the final mechanical properties of cement (Bentz *et al.*, 2009; Hu *et al.*, 2013). Regarding the pore solution, the w/c ratio influences the K, Na and alkali concentrations, while it slightly affects the concentrations of Si, Al, Ca and SO_4^{2-}. The concentrations of Ca and SO_4^{2-} are restricted due to the solubility limitations of $Ca(OH)_2$, and ettringite and AFm, respectively (Vollpracht *et al.*, 2015). Ca, Si, Al and OH^- concentrations are affected as the hydration proceeds and pH rises, as a result of the calcium sulphate depletion and precipitation of CH (Rothstein *et al.*, 2002).

The calorimetric curves of wPc at different w/c ratios during the first 24 hrs after mixing are shown in Fig. 5a. A slight influence of different w/c ratios on the wPc hydration kinetics at early ages is observed. As the w/c ratio increases, the degree of hydration increases and the maximum peak of heat release decreases due to the higher degree of dilution, and the availability of more space for the precipitation, nucleation and crystallisation of hydrated products (Xiong and van Breugel, 2001; Bentz *et al.*, 2009; Hu *et al.*, 2013; Scrivener *et al.*, 2015; Sedaghat, 2016; Wadsö *et al.*, 2017). As the hydration rate decreases, a delay in the acceleration period is observed due to the pore solution saturation being reached at longer times. However, the trends in all the calorimetric curves remain similar.

Fig. 5b shows the penetration depth of the Vicat needle into wPc at different w/c ratios. A faster initial time is observed, as the water content decreases, due to a lower degree of hydration, porosity and free water content make it easier to fill the space between the cement grains, producing a high-density cement paste (Stefanou and Larsinos, 1981; Atahan *et al.*, 2009; Marar and Eren, 2011).

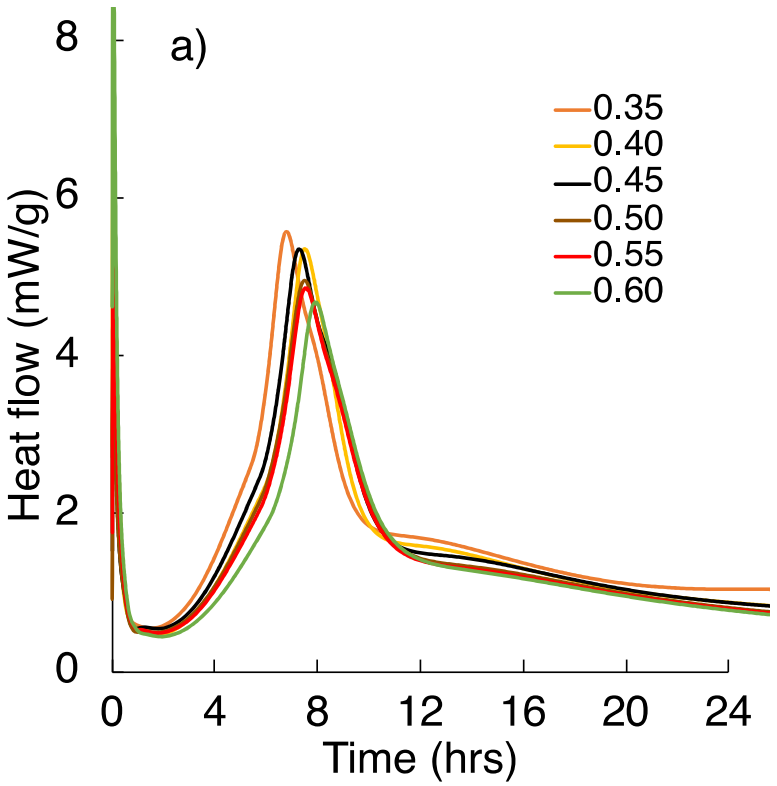
a)
Heat flow (mW/g)
Time (hrs)
0.35
0.40
0.45
0.50
0.55
0.60
0
2
4
6
8
0
4
8
12
16
20
24

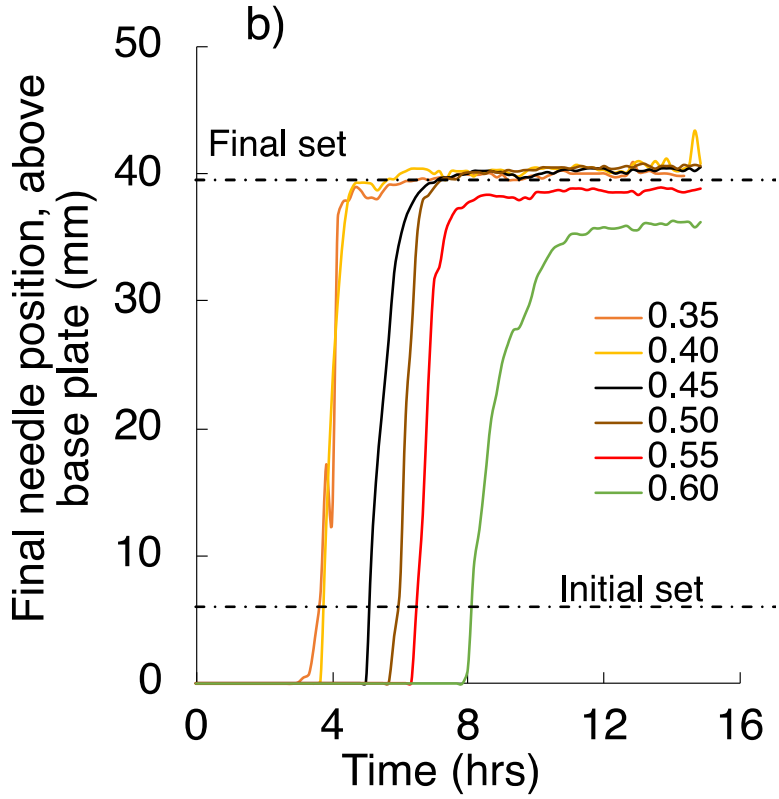
b)
Final needle position, above base plate (mm)
Time (hrs)
Final set
Initial set
0.35
0.40
0.45
0.50
0.55
0.60
0
10
20
30
40
50
0
4
8
12
16

Fig. 5. wPc at different w/c ratios: a) heat flow, b) Vicat determination of setting time.

The ACIS data, and specifically resistivity/conductivity measurements, of wPc hydrating at different w/c ratios during the first 24 hrs after mixing are shown in Fig. 6a-b. Fig. 6c-d show a different perspective of the wPc ACIS response at different w/c ratios, by representing the measurements in terms of resistance (Z' axis), and reactance (linked to capacitance; -Z'' axis), over time and frequency.

At early hydration periods (5 min), a semicircular arc of small impedance values at high frequency and low bulk resistance are observed due to the high conductivity of cement paste, which is attributed to the initial dissolution of alkali sulphate phases into the aqueous solution surrounding the cement grains (Whittington *et al.*, 1981; Xu *et al.*, 1993; Christensen *et al.*, 1994).

During the acceleration period, and as mentioned earlier, the impedance measurements at high frequency are affected by parasitic effects, obscuring the resistive and capacitive behaviour of the paste. The impedance measurements at high frequency are affected by some expected parasitic features from 3.5 to 8 hrs depending on the w/c ratio (Navi and Pignat, 1996; Taylor, 1997; Mehta and Monteiro, 2006; Renaudin *et al.*, 2015; Hewlett and Liska, 2019).

In the impedance measurements at high frequency, a delay in the rise of parasitic effects is observed as the cement water content increases (Fig. 6d). This is due to an increase of the dilution degree, the available space, the porosity of the system, and a decrease in the hydration rate (Gu *et al.*, 1995; Manchiryal and Neithalath, 2008; Neithalath and Jain, 2010). At this stage the pore solution is saturated or oversaturated with respect to $Ca(OH)_2$ (Rothstein *et al.*, 2002).

As the hydration process continues and the concentrations of Ca and SO_4^{2-} decrease, due to the precipitation of $Ca(OH)_2$ and ettringite, the impedance and bulk resistance values increase. Bulk resistance and reactance perturbations (at low frequency) are observed between 8 to 12 hrs, during which time the maximum heat release (end of acceleration period), final setting time, and the beginning and middle stages of the deceleration period take place (Cormack *et al.*, 1998; Barsoukov and Macdonald, 2005; Yuan *et al.*, 2010; Scrivener *et al.*, 2015).

At longer hydration ages (24 hrs), the calcium sulphate from the cement is fully consumed and, as the impedance and bulk resistance values increase, the parasitic effects show a decreasing tendency due to the reduction of free water content, low hydration rate and a more highly developed microstructure (Navi and Pignat, 1996; Taylor, 1997; Mehta and Monteiro, 2006; Renaudin *et al.*, 2015; Hewlett and Liska, 2019). At this point, the conductivity of the sample maintains a decreasing tendency and the effect of pH within the pore solution is smaller. This is attributed to the microstructural percolation and lower OH^-, SO_4^{2-} (controlled by AFm) concentrations in the pore solution. Also, as the w/c ratio decreases (Fig. 6b), the resistivity measurements increase due to a more refined pore size distribution and a lower free water content in the pores. Although the degree of hydration rises as the w/c ratio increases, lowering the alkali concentration and increasing the amount of hydrated products, higher resistivity values are obtained for pastes with lower w/c ratios. This demonstrates that the impedance response at this stage is mainly controlled by the percolation and pore size distribution of the microstructure (Fig. 7a-b), (Scuderi *et al.*, 1991; Zhutovsky and Kovler, 2009; Kwon *et al.*, 2010).

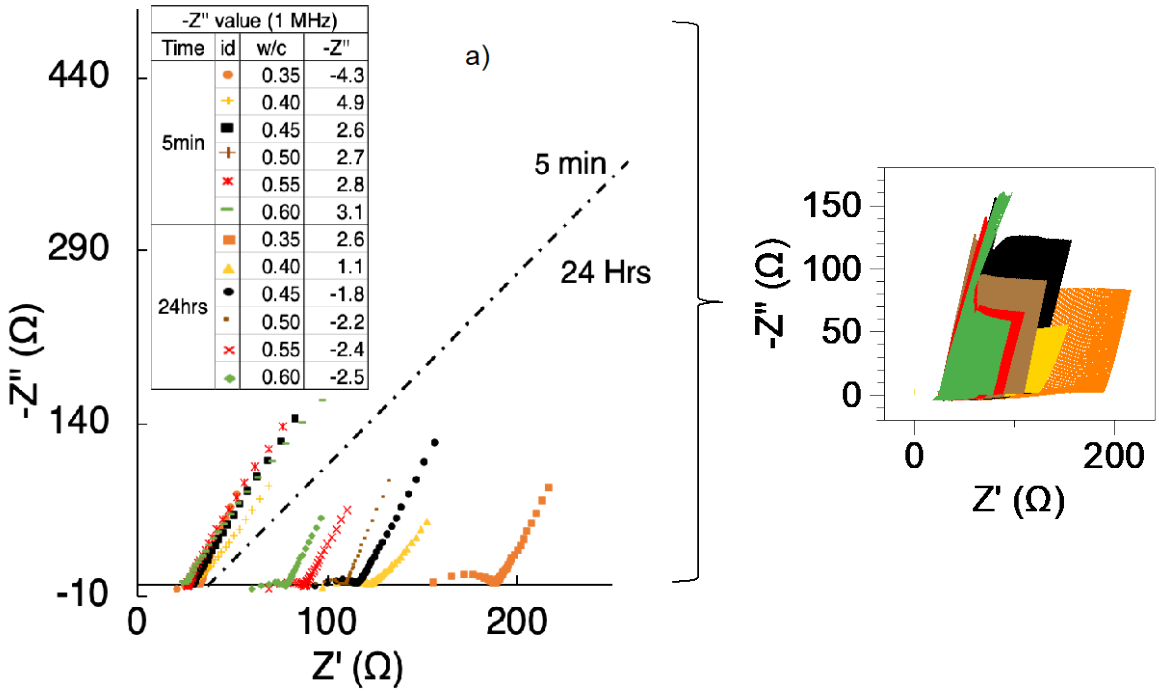
-Z'' value (1 MHz)
Time
id
w/c
-Z''
5min
0.35
-4.3
0.40
4.9
0.45
2.6
0.50
2.7
0.55
2.8
0.60
3.1
24hrs
0.35
2.6
0.40
1.1
0.45
-1.8
0.50
-2.2
0.55
-2.4
0.60
-2.5
a)
5 min
24 Hrs
440
290
140
-10
-Z'' (Ω)
0
100
200
Z' (Ω)
150
100
50
0
-Z'' (Ω)
0
200
Z' (Ω)

425

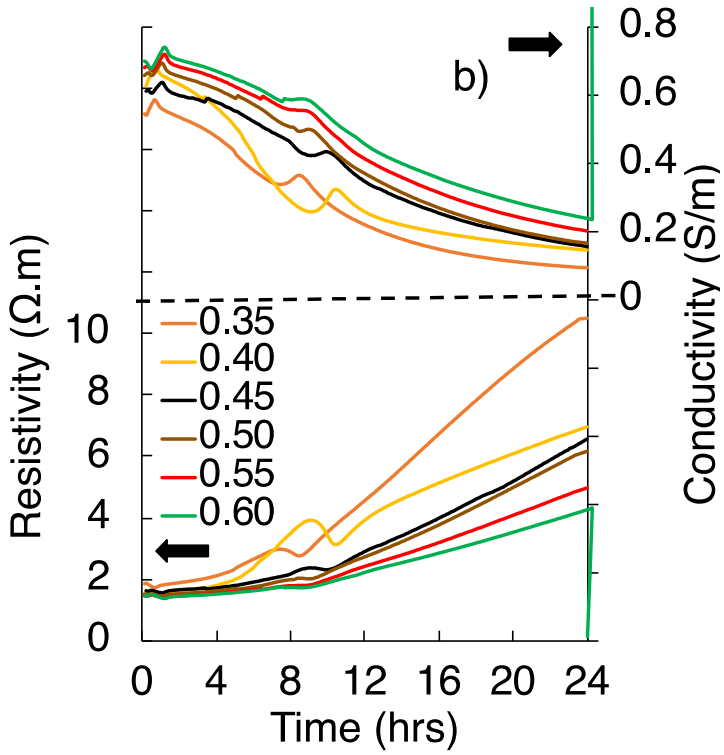
b)
Resistivity (Ω.m)
Conductivity (S/m)
Time (hrs)
0.35
0.40
0.45
0.50
0.55
0.60

426

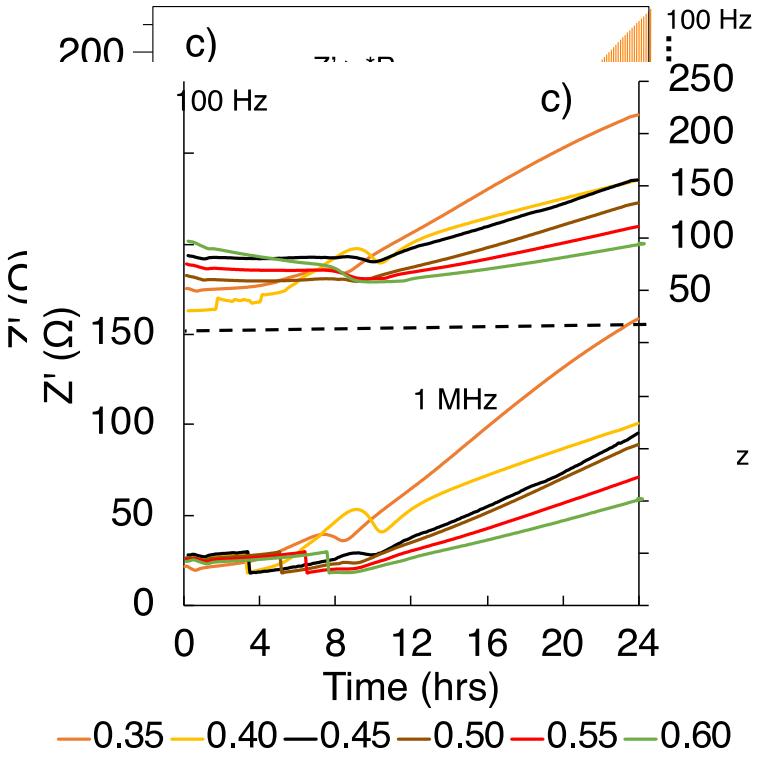
c)
100 Hz
1 MHz
Z' (Ω)
Time (hrs)
0.35
0.40
0.45
0.50
0.55
0.60

427

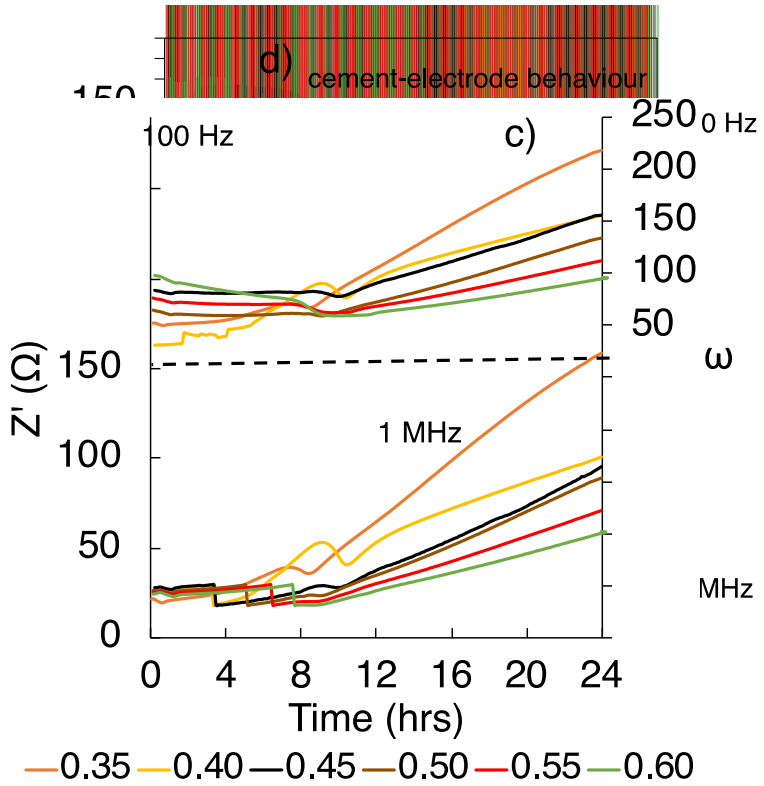

Fig. 6. ACIS response of wPc pastes with different w/c ratios as indicated in the legend, at 100 Hz and 1 MHz: a) Nyquist plots b) conductivity and resistivity, and at 100 Hz and 1 MHz c) real component, and d) imaginary component.

a) wPc (w/c:0.35) 24 hrs 50 μm

b) wPc (w/c:0.45) 24 hrs 50 μm

Fig. 7. SEM images of wPc pastes at 24 hrs after mixing: (a) w/c 0.35 (b) w/c: 0.45.

The wPc hydrated at w/c: 0.35 (Fig. 7a) shows a slightly denser pore size distribution, and higher percolation of the microstructure, while wPc at w/c: 0.45 (Fig. 7b) shows a higher capillary porosity and lower hydrated product content.

4.3 Effects of sand addition

Sand is used in cementitious materials as an inert aggregate material that behaves as a filler, changing the mechanical properties, alkali concentration in the pore solution, kinetics of reaction, and the development of the microstructure. Also, the use of aggregates such as sand can influence the air voids content, pore size distribution and pore volume of mortars and concretes (Dong *et al.*, 2014; Hewlett and Liska, 2019).

At early ages, the pore solution of mortars depends mainly on the alkali content in cement and the free water content in the system affecting the NaOH and KOH concentration and the rate of hydration and kinetics of reactions, respectively. At longer ages, the use of sand slightly affects the OH^- concentration and reduces the pH due to a dilution effect (Owsiak, 2004; Mehta and Monteiro, 2006; Buckley *et al.*, 2007).

Fig. 8a shows the calorimetric curves of wPc at different sand replacement levels during the first 24 hrs after mixing. As the sand replacement level is increased, a delaying effect on the hydration process, related to dilution associated to a filler effect, is observed. Also, the decrease in the amount of reactive constituents per volume of material as a result of the addition of sand reduces the heat release, and brings some change in the microstructural development due to nucleation and other effects (Zeghichi *et al.*, 2014; Topič and Prošek, 2017).

The appearance of C_3S and sulphate depletion peaks at lower heat and the same times after mixing, due to the hydration kinetics of cement, are observed. Sand is considered to be an inert material that does not affect the chemistry of cement; however, it has a notable impact on the hydration process by increasing the space among the cement particles, and by inducing an acceleration of the hydration reactions. The sulphate depletion peak is more noticeable for mortars than pastes due to a delayed conversion of ettringite into monosulphate (Haines, 2002; Xu *et al.*, 2010; Frølich *et al.*, 2016).

The penetration depth of the Vicat needle into wPc pastes at different sand replacement levels and w/c of 0.45 is observed in Fig. 8b. As the amount of wPc is decreased, the initial and final setting times of mortar are reached at longer times, resulting in a delay in the hydration process, a lower hydration degree, and some change in the hydration kinetics of the system. Mortars with 40-60% sand content show a slowed setting behaviour, attributed to a low cement and water content and high content of pores and air voids in the microstructure, leading to a decrease in strength. These effects are attributed to the sand water uptake, and lower cement and water content (Suresh and Revathi, 2016; Bouasker *et al.*, 2017).

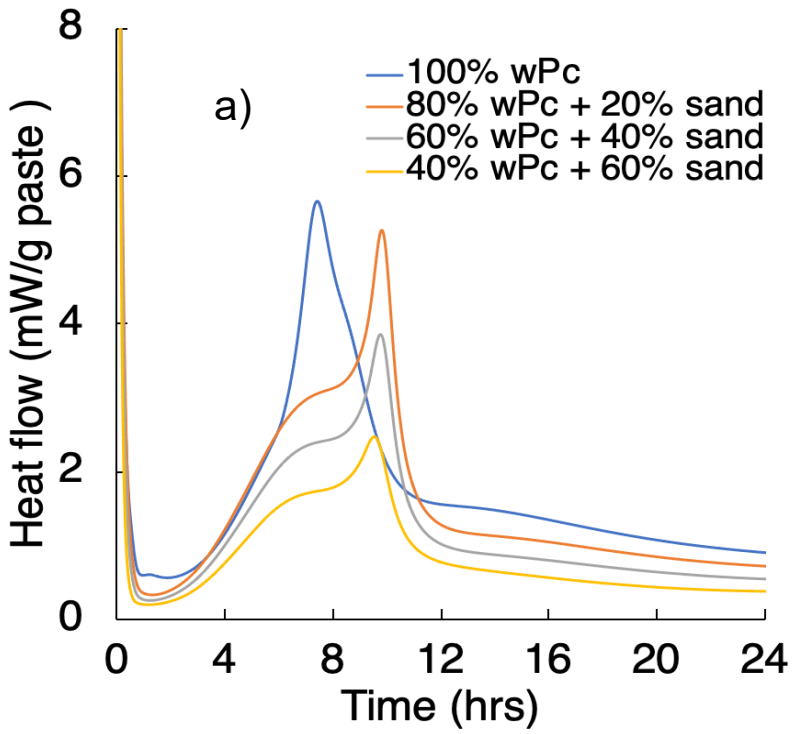
a)
100% wPc
80% wPc + 20% sand
60% wPc + 40% sand
40% wPc + 60% sand
Heat flow (mW/g paste)
Time (hrs)
0
2
4
6
8
0
4
8
12
16
20
24

484

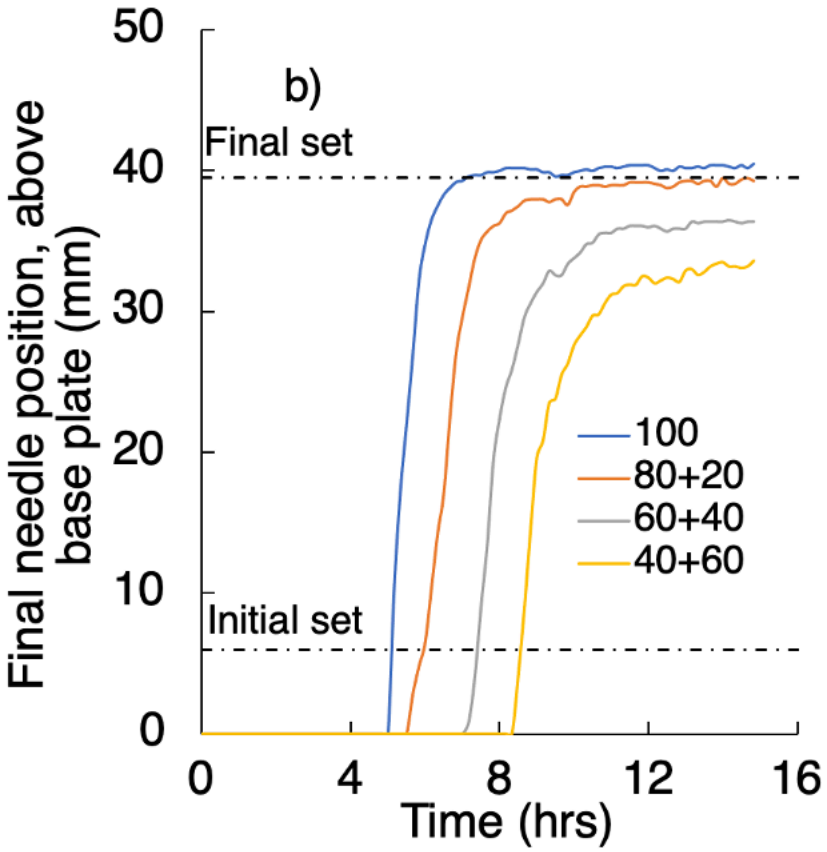

Fig. 8. wPc hydration at different sand replacement levels as indicated in the legend: a) heat flow (normalised to total sample mass), b) Vicat determination of setting time.

Fig. 9a-d shows the wPc ACIS, resistivity/conductivity, and impedance response in terms of resistance and reactance over time and frequency, at different sand replacement levels, during the first 24 hrs after mixing.

At early ages and comparing wPc paste to mortars (Fig. 9a), the results show an increasing tendency of the impedance and parasitic effects as the sand replacement level increases. This effect is attributed to an increase in the conductivity of the aqueous fluid surrounding the cement grains (Tumidajski, 1996; He *et al.*, 2017). There is also a filler effect produced by the addition of sand which increases the growth and the nucleation

sites for hydrated products. In Fig. 9b the bulk resistivity of the mortar increases due to a lower amount of C_3A per unit volume of material and fewer available wPc grains to react with water, leading to an increase in the dissolution rate of anhydrous compounds and the formation of hydration products around the cement particles (mainly C-A-$\bar{S}$-H phases, and some early C-S-H). This response confirms that the addition of sand has a significant dilution and electrical insulating effect during the microstructural development of mortars, causing a decrease in their electrical conductivity (Brantervik and Niklasson, 1991; Tumidajski, 1996). During the dormant period, as the amount of sand is increased, the impedance response in terms of bulk resistance (Fig. 9c) shows an increasing tendency at low and high frequency, confirming the impact of the mortar microstructure on the impedance response (He *et al.*, 2017).

As wPc is replaced by sand, the reactance decreases at low frequency, and increases at high frequency, and it is also observed that the parasitic effects increase and emerge at earlier times (Fig. 9d). These behaviours are probably related to a decrease in the charge transfer resistance as a result of a higher ionic strength and a sand filler effect, demonstrating the impact on the hydration kinetics produced by the addition of sand (Feldman, 1986; McCarter and Garvin, 1989; Bu *et al.*, 2017).

At the beginning of the acceleration period, there is no change in the appearance rate of the main C_3S hydration peak (Fig. 8), but the mortars show a similar increasing trend in which the bulk resistance values are higher than the values for wPc (Fig. 9). This is attributed to a microstructural change produced by the sand-cement interface which affects the air voids and porosity of the mortars (Fig. 10a-b), leading to an increase in resistivity of the sample (Cao and Chung, 2004).

At the end of the acceleration period, the sulphate depletion peaks of mortars at different sand addition levels are observed at similar times, while the resistivity/conductivity measurements show a perturbation between 10-11 hrs that is delayed as the sand level is increased. This perturbation is not only related to the

maximum release of heat (sulphate depletion peak, (Fig. 8a) but also to the impact of sand on the microstructural development, deposition of hydrated products such as CH, and pore size distribution and content (Bu *et al.*, 2017).

At longer ages, mortars show similar impedance behaviour in which a bulk semicircular arc of higher resistance is obtained. However, the parasitic effects in the ACIS measurements are reduced at 20% to 40% sand replacement levels. Higher sand replacement (60%) shows a greater parasitic effect. This is due to an interfacial effect in which the total porosity, the pore size and the pore distribution increase at high sand replacement levels (Feldman, 1986).

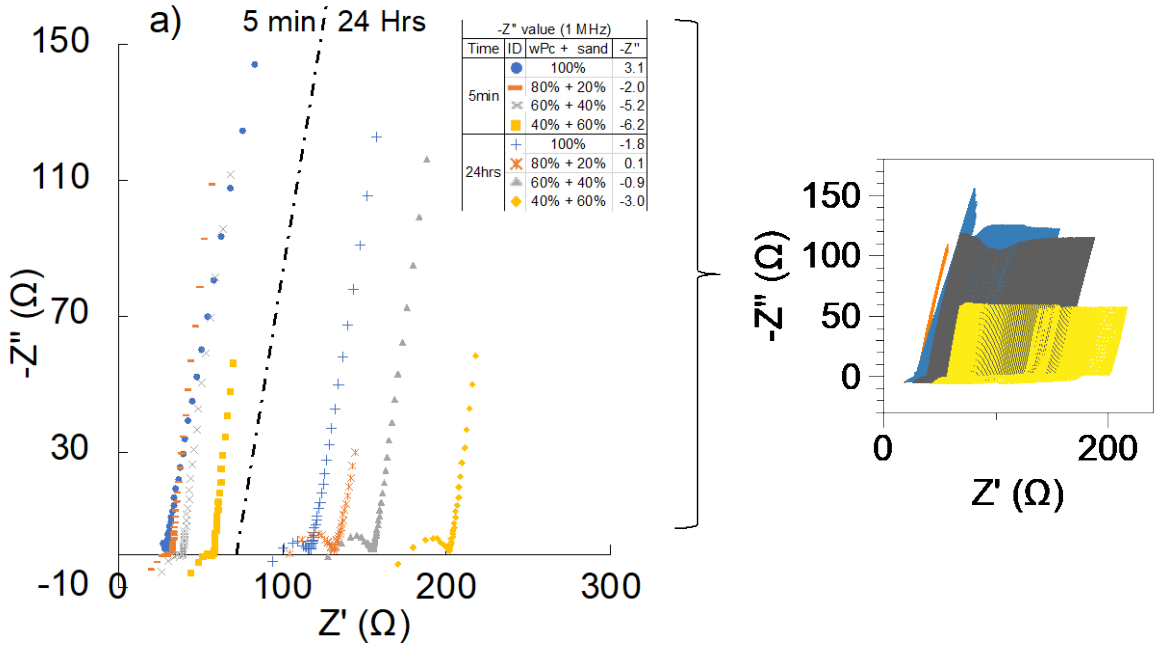
a)
5 min / 24 Hrs
-Z" value (1 MHz)
Time | ID | wPc + sand | -Z"
5min | 100% | 3.1
80% + 20% | -2.0
60% + 40% | -5.2
40% + 60% | -6.2
24hrs | 100% | -1.8
80% + 20% | 0.1
60% + 40% | -0.9
40% + 60% | -3.0
-Z" (Ω)
Z' (Ω)
150
110
70
30
-10
0
100
200
300
150
100
50
0
200

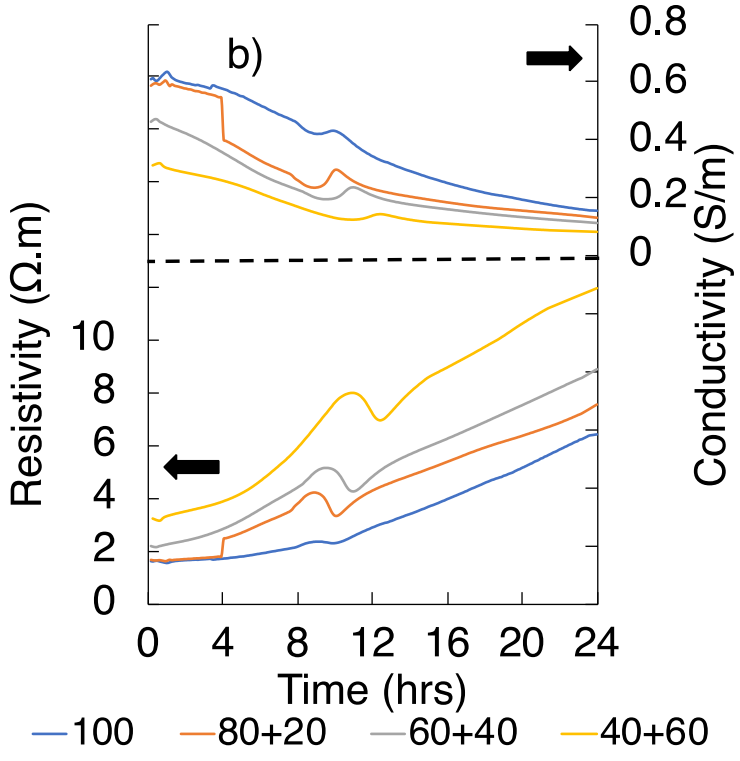
b)
Resistivity (Ω.m)
Conductivity (S/m)
Time (hrs)
0.8
0.6
0.4
0.2
0
10
8
6
4
2
0
0
4
8
12
16
20
24
100
80+20
60+40
40+60

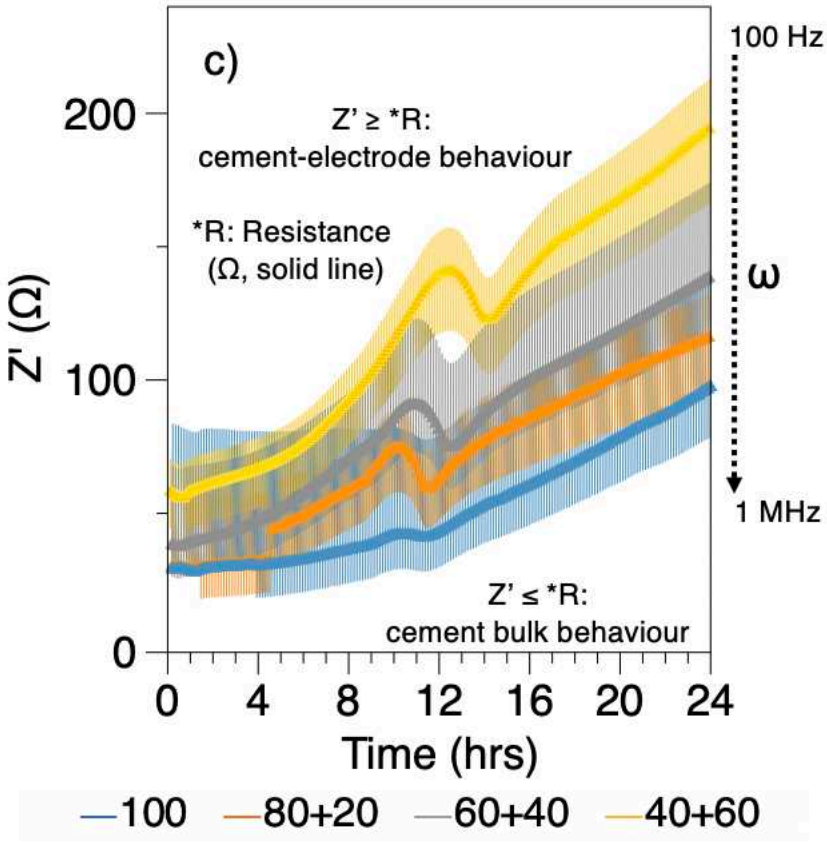
c)
Z' ≥ *R:
cement-electrode behaviour
*R: Resistance
(Ω, solid line)
Z' ≤ *R:
cement bulk behaviour
100 Hz
ω
1 MHz
Z' (Ω)
200
100
0
0
4
8
12
16
20
24
Time (hrs)
100
80+20
60+40
40+60

542

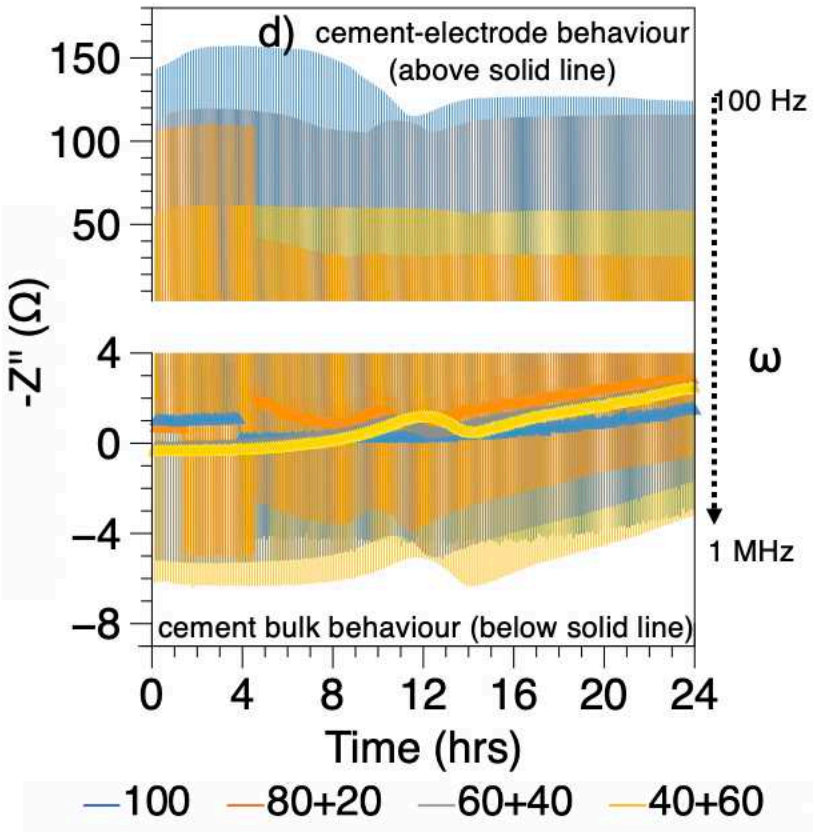

Fig. 9. ACIS response of wPc pastes at different sand replacement levels as indicated in the legend: a) Nyquist plots, b) conductivity and resistivity, and at 100 Hz and 1 MHz c) real component, and d) imaginary component.

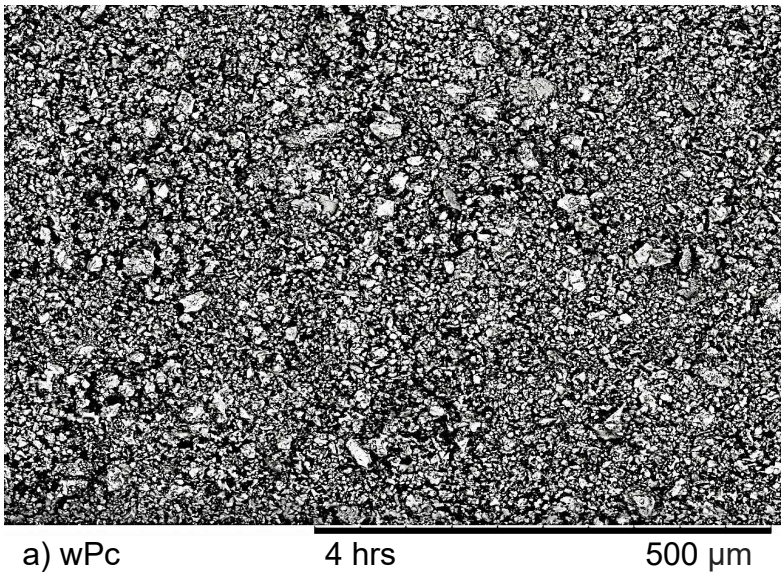

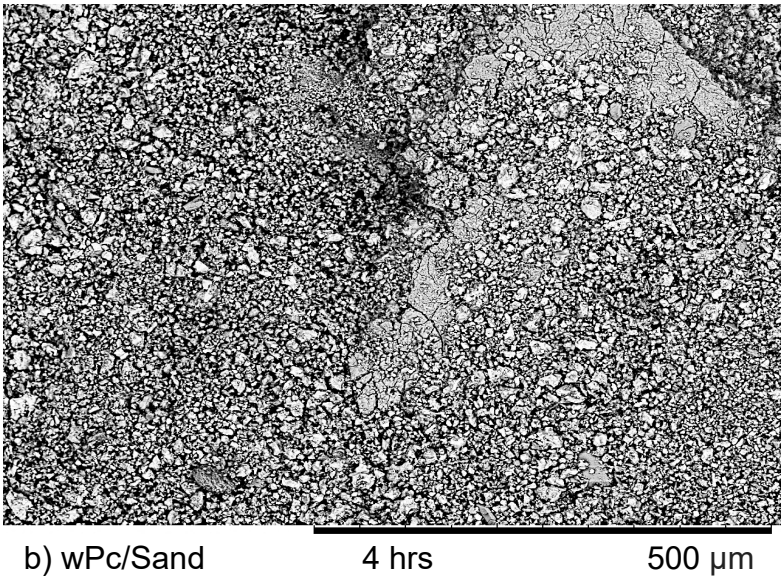

Fig. 10. SEM images of wPc paste (a) and mortar (b) at 4 hrs after mixing.

4.4 Anhydrite addition to cement

The reaction of C_3A during the cement hydration process is of great importance, as C_3A in contact with water reacts faster than other clinker phases, leading (if it is not controlled) to the formation of calcium aluminate products, rapid release of heat, and potentially quick/flash setting of cement if it is not controlled. To prevent this, the C_3A reaction is slowed down by the addition of a few wt.% of calcium sulphate sources such as gypsum ($CaSO_4 \cdot 2H_2O$), anhydrite ($CaSO_4$ or $C\bar{S}$) or hemihydrate ($CaSO_4 \cdot 0.5H_2O$) which are usually added during cement manufacturing to retard the C_3A hydration (≈ 2%) (Ramachandran, 1995; Mehta and Monteiro, 2006; Hewlett and Liska, 2019).

The presence of these of the calcium sulphate can regulate the setting of Portland cement and control the sulphate concentration in the cement system, by changing the kinetics of reaction during hydration. The amount of calcium sulphate required for a particular cement will depend on the amount of sulphate and C_3A in the clinker. An excessive addition of calcium sulphate can cause a false set and, at early ages, a slight influence on the pore solution. Meanwhile, the rate at which Al^{3+} ions enter the pore solution and the hydrated product formation (i.e. ettringite and AFm) are strongly affected by the amount and source of calcium sulphate (Pelletier-Chaignat *et al.*, 2011; McCague *et al.*, 2014).

The calorimetric curves of wPc at different anhydrite replacement levels during the first 24 hrs after mixing are shown in Fig. 11a. At small replacements (0.5-1%) of anhydrite in wPc pastes, the data show a similar trend to wPc paste. However, in the hydration process there is a retardation effect attributed to the slower dissolution of anhydrite, in which the release of heat decreases as the amount of anhydrite is increased. At high anhydrite replacement levels (10%) the calorimetric curve shows different behaviour, in which the heat release rate decreases significantly and the deceleration period increases in correlation to the sulphate depletion (Novotný *et al.*, 2016).

The dormant and acceleration periods, and the maximum exothermic peak, have similar heat evolution rate values in samples with 0 to 1% anhydrite content, Fig. 11a. At

10% of anhydrite replacement, the heat evolution rate values decrease due to an early and higher formation of AFt phase on cement grains (Xu *et al.*, 2012; Jen *et al.*, 2017). In the deceleration period, the heat evolution rate increases as the anhydrite replacement level increases. These effects suggest that the setting is prolonged as anhydrite amount increases, which is attributed to the anhydrite retardation effect on the reaction of C_3A and C_3S, the precipitation of ettringite and nucleation of AFm phases, and a reduction of the available space for reaction due to the amount of ettringite produced (Tydlitát and Tesárek, 2008; Xu *et al.*, 2012; Bentz *et al.*, 2016; Novotný *et al.*, 2016; Kumar *et al.*, 2017).

The penetration depth of the Vicat needle into wPc pastes at different anhydrite replacement levels is observed in Fig. 11b. The partial replacement of cement by anhydrite has only a slight effect on the initial setting time, and no false setting is observed even at the highest level of anhydrite addition. On the other hand, a higher retardation effect is observed in the final setting time as the amount of anhydrite is increased. The results agree with the thermochemistry data, attributed to the retardation of C_3A retardation effect due to the addition of anhydrite which produces AFt and prolongs the sulphate depletion time. This effect is followed by the reaction of CH and ettringite with the remaining C_3A content, producing AFm phases (Bullard *et al.*, 2011; Ylmén, 2013).

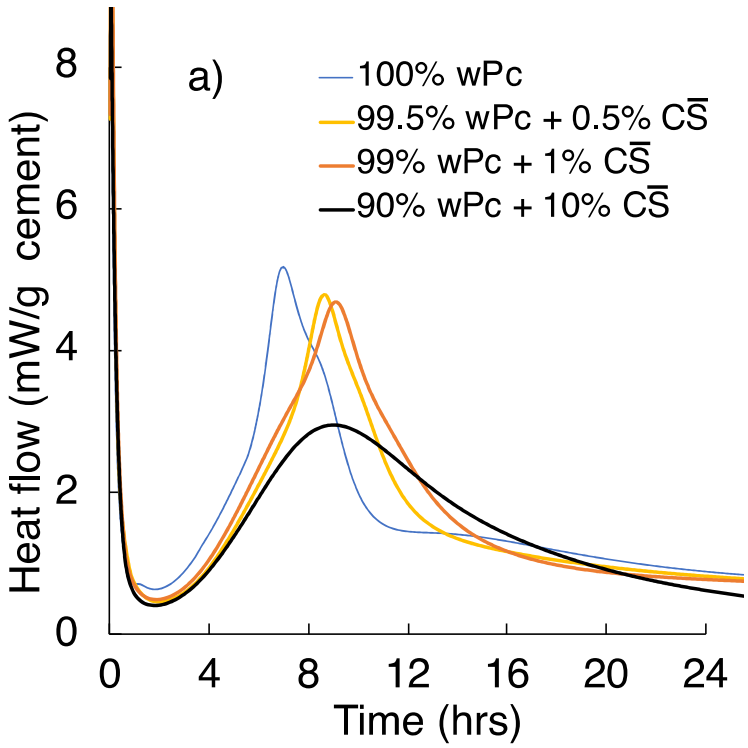
a)
100% wPc
99.5% wPc + 0.5% CS̄
99% wPc + 1% CS̄
90% wPc + 10% CS̄
Heat flow (mW/g cement)
0
2
4
6
8
0
4
8
12
16
20
24
Time (hrs)

607

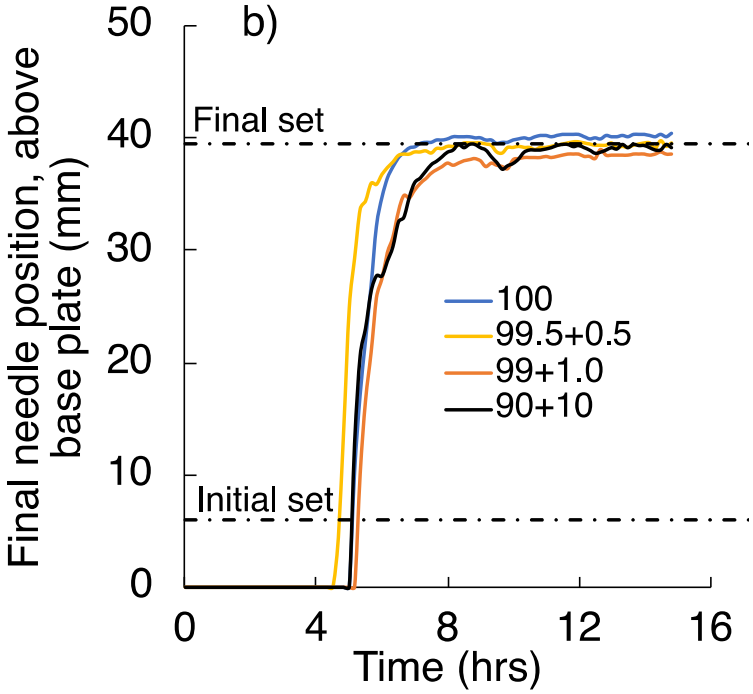
b)
Final set
Initial set
100
99.5+0.5
99+1.0
90+10
Final needle position, above base plate (mm)
0
10
20
30
40
50
0
4
8
12
16
Time (hrs)

608

609

Fig. 11. wPc hydration at different anhydrite ($C\bar{S}$) replacement levels. as indicated in the legend: a) heat flow, b) Vicat determination of setting time.

Fig. 12a-d show the wPc ACIS data, resistivity/conductivity, and the impedance response in terms of resistance and reactance over time and frequency at different anhydrite replacement levels during the first 24 hrs after mixing.

At early ages, the conductivity/resistivity (Fig. 12b), and impedance behaviour (Fig. 12a) show similar behaviour in all samples. The -Z'' values decrease as the anhydrite replacement level increases, showing a parasitic effect at 10% anhydrite replacement, and this effect needs further investigation. At high frequency and at approximately 1 hr after mixing, a perturbation in the conductivity, and in the real and imaginary impedance components, (Fig. 12c-d) is observed. Comparing these results with the thermochemical data, these perturbations are attributed to the beginning of the dormant period. This effect is followed by a decreasing tendency in the conductivity as the anhydrite replacement increases; at 1% anhydrite replacement, the data show a sharp and higher conductivity drop (García-Maté *et al.*, 2015).

At approximately 2-4 hrs after mixing, the -Z'' axis data show a sudden appearance of parasitic effects which increase as the replacement of anhydrite increases. The paste with 10% anhydrite is the first sample which shows this behaviour due to a dissolution rate decrease, followed by the paste with 0.5% anhydrite, while the paste with 1% anhydrite has a behaviour similar to wPc paste. The sudden appearance of parasitic effects is correlated to the beginning of the acceleration period.

The rate of dissolution of anhydrite and reaction of C_3A are accelerated as the calcium sulphate content increases and the dissolution of C_3S and C_2S begins. However, for all samples in the dormant period and the beginning of the acceleration period, the calorimetric curves (Fig. 11a) show a similar trend and the effect of anhydrite is not evident (Quennoz, 2011; García-Maté *et al.*, 2015; Xiong *et al.*, 2016). An increasing tendency in the conductivity measurements is observed 6 hours after mixing; this effect

is attributed to greater formation of AFt due to the depletion of anhydrite, which decreases at later ages (Pelletier-Chaignat *et al.*, 2011).

Around 8-12 hrs after mixing, at the end of the acceleration period and during the deceleration period, perturbations in resistivity and impedance values in terms of the bulk resistance and reactance (Z' and -Z'' axis) are observed. However, the thermochemical and penetration displacement results are not enough to support full identification of the behaviour of the impedance spectra as wPc is replaced by anhydrite. Regarding the concentration of the ionic species in the pore solution and microstructural features at this stage of hydration, a more detailed investigation is needed to complement the interpretation of the impedance behaviour of wPc at different anhydrite replacement levels.

At longer ages and comparing to the ACIS response of wPc paste, the impedance values decrease for pastes with 0.5% and 1% anhydrite, and the parasitic effect increases as the replacement level increases. The sample with 10% anhydrite shows an increase of the impedance values and a higher resistivity bulk semicircular arc. Samples with 1% and 10% anhydrite replacement show conductivity values lower than those of wPc paste, while the 0.5% anhydrite sample shows a conductivity slightly higher than those of wPc paste. To understand and correlate the anhydrite replacement effect on the impedance behaviour, thermochemistry and initial and final setting times, further investigation, based on microstructural changes, is needed.

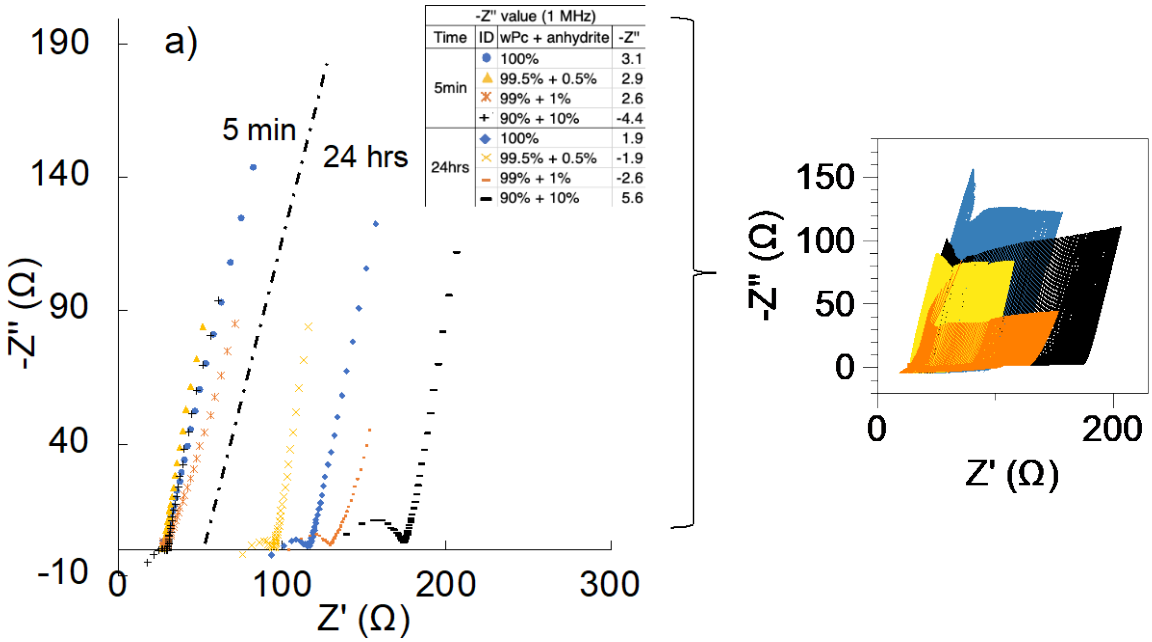
a)
5 min
24 hrs
-Z" value (1 MHz)
Time | ID | wPc + anhydrite | -Z"
5min | 100% | 3.1
5min | 99.5% + 0.5% | 2.9
5min | 99% + 1% | 2.6
5min | 90% + 10% | -4.4
24hrs | 100% | 1.9
24hrs | 99.5% + 0.5% | -1.9
24hrs | 99% + 1% | -2.6
24hrs | 90% + 10% | 5.6
-Z" (Ω)
Z' (Ω)
190
140
90
40
-10
0
100
200
300
150
100
50
0
200

663

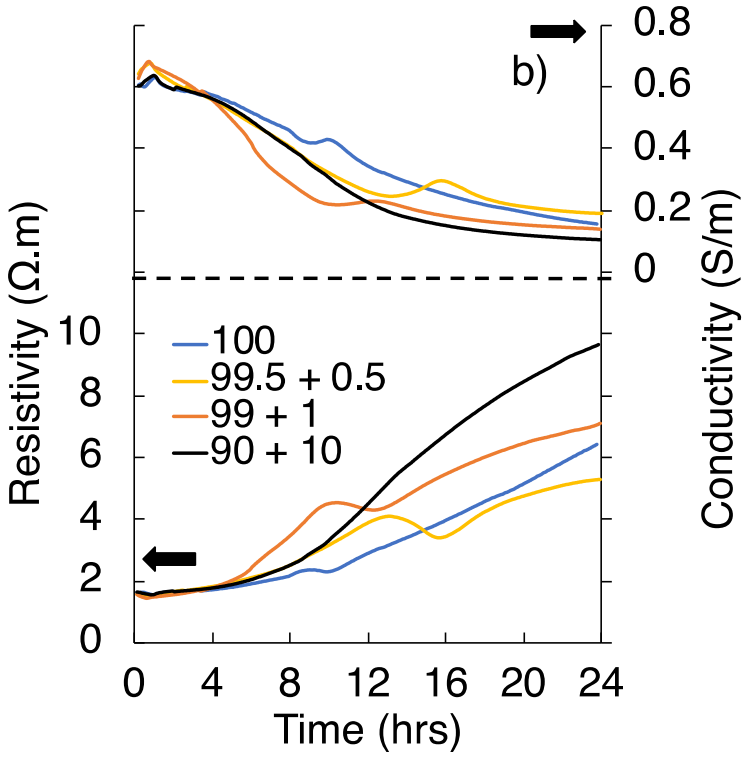
b)
Resistivity (Ω.m)
Conductivity (S/m)
Time (hrs)
100
99.5 + 0.5
99 + 1
90 + 10
0.8
0.6
0.4
0.2
0
10
8
6
4
2
0
4
8
12
16
20
24

664

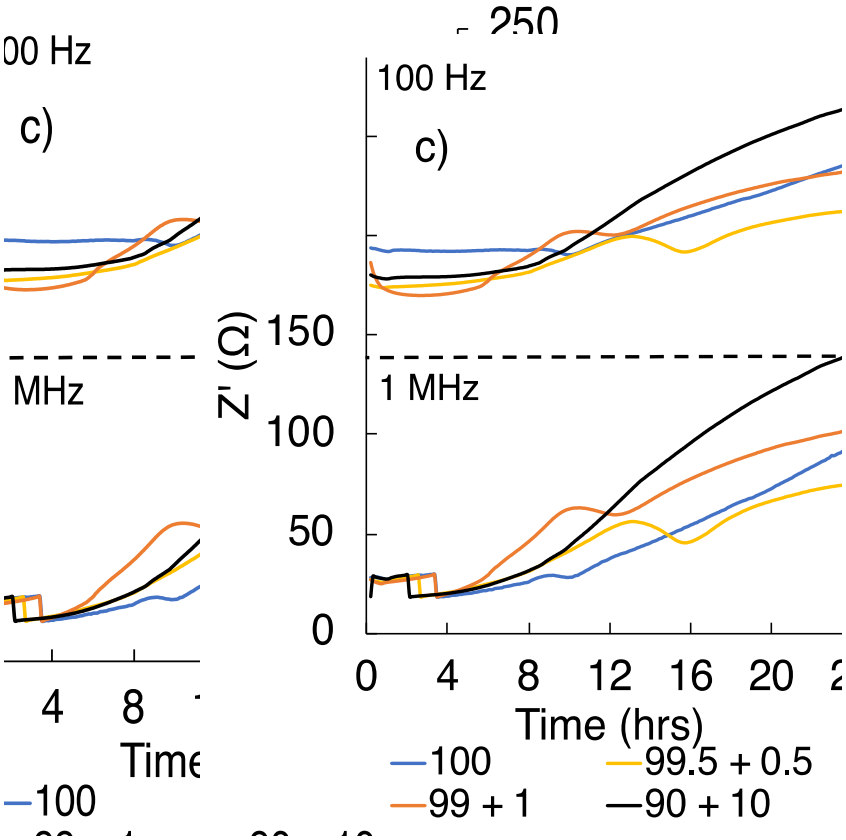
100 Hz
c)
1 MHz
Z' (Ω)
150
100
50
0
0
4
8
12
16
20
Time (hrs)
100
99.5 + 0.5
99 + 1
90 + 10

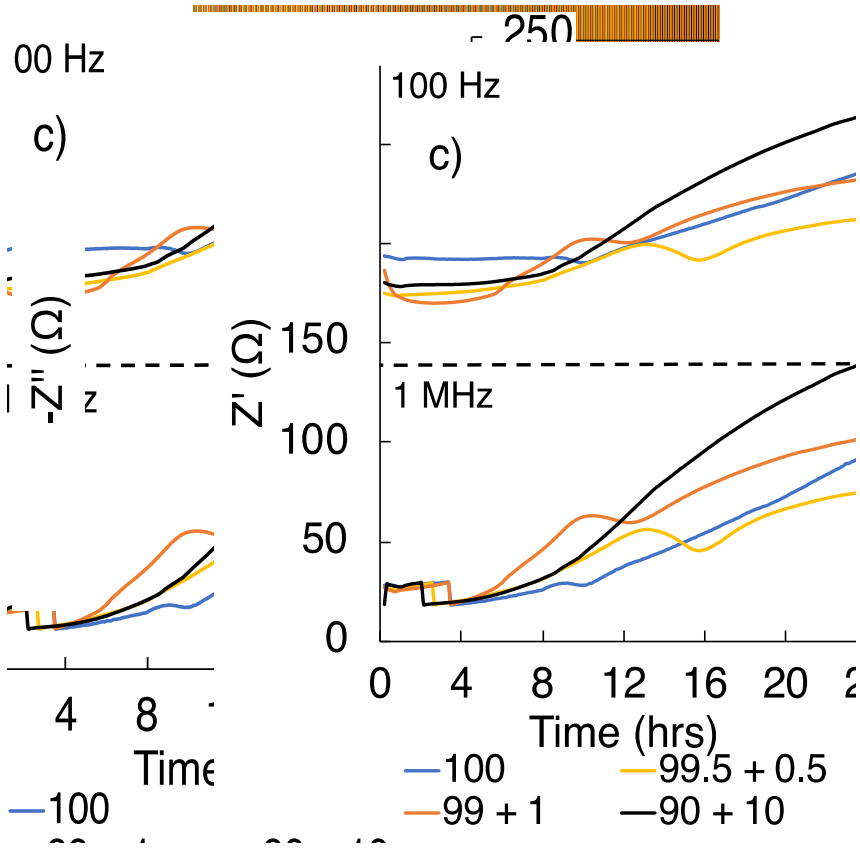

Fig. 12. ACIS response of wPc pastes at different anhydrite replacement levels as indicated in the legend: a) Nyquist plots, b) conductivity and resistivity, and at 100 Hz and 1 MHz c) real component, and d) imaginary component.

5. Conclusions

In this investigation different techniques have been used to assess, during the first 24 hrs after mixing, the electrochemical response and the microstructural development of Portland cement at different w/c ratios and different sand and anhydrite replacement levels. The experimental results highlighted the following conclusions:

- The thermochemistry results show only a slight variation between the heat flows measured at different w/c ratios. Conversely, the ACIS measurements show a significant variation, in which the appearance of parasitic effects on the impedance measurements at high frequency can be correlated to the initial setting time.
- Perturbations in the electrical conductivity response are attributed to the dissolution of the clinker phases, and the precipitation of C-S-H, correlates with the thermochemistry results.
- The decreasing conductivity trends obtained as a function of time are related to the microstructural development of cementitious systems (hydrated product formation and disconnection of pores) and consumption of water/pore fluid.
- Microstructural changes during hydration are produced by altering the chemistry of the cementitious paste or mortar and can be observed via changes in the electrical resistivity and the impedance behaviour. These changes are correlated with some features in the thermochemistry and setting time results.
- Cement conductivity, resistivity and impedance behaviour, as a function of time, correspond to the results of previous investigations.
- The results show that ACIS measurement can be implemented at early cement hydration ages (≤24 h) by using the proposed custom-cell design to reduce parasitic effects at high frequencies (Sosa Gallardo and Provis, 2020). Benchmark techniques demonstrated that ACIS is capable to assess the impact of the ionic strength characteristics of the pore solution, the thermochemical and the microstructural changes during cement hydration. However, further experimental work is required to extend and validate the approaches for broader application.

In summary, despite of the fact that at early ages impedance measurements are affected by parasitic effects due to a highly conductive cement state and a low degree of microstructural development, the study of cement hydration and the influence of admixtures can be accomplished by ACIS. However, to obtain more robust impedance

data interpretation, the appearance of parasitic effects on ACIS measurements and microstructural characterisation need further investigation.

Acknowledgements

This study was funded by the National Council on Science and Technology (CONACYT), and the European Union through the 7th Framework Programme (European Research Council Starting Grant #335928).

References

ASTM International (2017) *ASTM C1679 -17. Standard practice for measuring hydration kinetics of hydraulic cementitious mixtures using isothermal calorimetry*. West Conshohocken, PA.

Atahan, H.N., Oktar, O.N. and Taşdemir, M.A. (2009) 'Effects of water-cement ratio and curing time on the critical pore width of hardened cement paste', *Construction and Building Materials*, 23(3), pp. 1196–1200.

Azarsa, P. and Gupta, R. (2017) 'Electrical resistivity of concrete for durability evaluation: A review', *Advances in Materials Science and Engineering*, 2017, #8453095

Backe, K.R., Lile, O.B. and Lyomov, S.K. (2001) 'Characterizing curing cement slurries by electrical conductivity', *SPE Drilling & Completion*, pp. 201–207.

Barsoukov, E. and Macdonald, J.R. (2005) *Impedance spectroscopy theory, experiment, and applications*. 2nd ed. Hoboken, New Jersey: Wiley-Interscience.

Bentz, D., Zunino, F. and Lootens, D. (2016) 'Chemical vs. physical acceleration of cement hydration', *Concrete International*, 38(11), pp. 37–44.

Bentz, D.P., Peltz, M.A. and Winpigler, J. (2009) 'Early-age properties of cement-based Materials. II: Influence of water-to-cement ratio', *Journal of Material in Civil Engineering*, 21(9), pp. 512–517.

Bligh, M.W., D'Eurydice, M.N., Lloyd, R.R. Arns, C.H. and Waite, T.D. (2016) 'Investigation of early hydration dynamics and microstructural development in ordinary

Portland cement using ^{1}H NMR relaxometry and isothermal calorimetry', *Cement and Concrete Research*, 83, pp. 131–139.

Bouasker, M., Mounanga, P., Turcry, P., Loukili, A. and Khelidj, A. (2017) 'Chemical shrinkage of cement pastes and mortars at very early age: Effect of limestone filler and granular inclusions', *Cement and Concrete Composites*, 30(1), pp. 13-22.

Brantervik, K. and Niklasson, G.A. (1991) 'Circuit models for cement based materials obtained from impedance spectroscopy', *Cement and Concrete Research*, 21, pp. 496–508.

Brouwers, H.J.H. and Van Eijk, R.J. (2003) 'Alkali concentrations of pore solution in hydrating OPC', *Cement and Concrete Research*, 33(2), pp. 191–196.

Bu, J., Tian, Z., Zheng, S. and Tang, Z. (2017) 'Effect of sand content on strength and pore structure of cement mortar', *Journal Wuhan University of Technology, Materials Science Edition*, 32(2), pp. 382–390. doi:10.1007/s11595-017-1607-9.

Buckley, L.J., Carter, M.A., Wilson, M.A. and Scantlebury, J.D. (2007) 'Methods of obtaining pore solution from cement pastes and mortars for chloride analysis', *Cement and Concrete Research*, 37(11), pp. 1544–1550. doi:10.1016/j.cemconres.2007.08.009.

Bullard, J.W., Jennings, H.M., Livingston, R.A., Nonat, A., Scherer, G.W., Schweitzer, J.S., Scrivener, K.L. and Thomas, J.J. (2011) 'Mechanisms of cement hydration', *Cement and Concrete Research*, 41(12), pp. 1208–1223.

Cao, J. and Chung, D.D.L. (2004) 'Microstructural effect of the shrinkage of cement-based materials during hydration, as indicated by electrical resistivity measurement', *Cement and Concrete Research*, 34, pp. 1893–1897.

Caruso, F., Mantellato, S., Palacios, M. and Flatt, R.J. (2017) 'ICP-OES method for the characterization of cement pore solutions and their modification by polycarboxylate-based superplasticizers', *Cement and Concrete Research*, 91, pp. 52–60. doi:10.1016/j.cemconres.2016.10.007.

Christensen, B.J., Coverdale, T., Olson, R.A., Ford, S.J., Garboczi, E.J., Jennings, H.M. and Mason, T.O. (1994) 'Impedance spectroscopy of hydrating cement-based materials: measurement, interpretation, and application', *Journal of the American Ceramic Society*, 77(11), pp. 2789–2804.

Cormack, S.L., Macphee, D.E. and Sinclair, D.C. (1998) ‘An AC impedance spectroscopy study of hydrated cement pastes’, *Advances in Cement Research*, 10(4), pp. 151–159.

Cruz, J.M., Payá, J., Lalinde, L.F. and Fita, I.C. (2011) ‘Evaluación de las propiedades eléctricas de morteros de cemento con puzolanas’, *Mater. Constr.*, 61(301), pp. 7–26.

Cruz, J.M., Fita, I.C., Soriano, L., Payá, J. and Borrachero, M.V. (2013) ‘The use of electrical impedance spectroscopy for monitoring the hydration products of Portland cement mortars with high percentage of pozzolans’, *Cement and Concrete Research*, 50, pp. 51–61.

Dewah, H.A.F., Austin, S.A. and Maslehuddin, M. (2002) ‘Effect of cement alkalinity on pore solution chemistry and chloride-induced reinforcement corrosion’, *ACI Materials Journal*, 97(3), pp. 227–233.

Dong, B, Qiu, Q., Xiang, J., Huang, C., Xing, F. and Han, N. (2014) ‘Study on the carbonation behavior of cement mortar by electrochemical impedance spectroscopy’, *Materials*, 7, pp. 218–231. doi:10.3390/ma7010218.

Dotelli, G. and Mari, C.M. (2001) ‘The evolution of cement paste hydration process by impedance spectroscopy’, *Materials Science and Engineering*, 303, pp. 54–59.

Feldman, R.F. (1986) ‘The effect of sand/cement ratio and silica fume on the microstructure of mortars’, *Cement and Concrete Research*, 16, pp. 31–39. doi:10.1360/zd-2013-43-6-1064.

Frølich, L., Wadsö, L. and Sandberg, P. (2016) ‘Using isothermal calorimetry to predict one day mortar strengths’, *Cement and Concrete Research*, 88, pp. 108–113.

García-Maté, M., de la Torre, A.G., León-Reina, L., Losilla, E.R., Aranda, M.A.G. and Santacruz, I. (2015) ‘Effect of calcium sulfate source on the hydration of calcium sulfoaluminate eco-cement’, *Cement and Concrete Composites*, 55, pp. 53–61.

Gerstig, M. and Wadsö, L. (2010) ‘A method based on isothermal calorimetry to quantify the influence of moisture on the hydration rate of young cement pastes’, *Cement and Concrete Research*, 40(6), pp. 867–874.

Haines, P.J. (2002) *Principles of thermal analysis and calorimetry*. Cambridge, England.

He, F., Wang, R., Shi, C., Zhang, R., Chen, C., Lin, L. and An, X. (2017) ‘Differential

analysis of AC impedance spectroscopy of cement-based materials considering CPE behavior', *Construction and Building Materials*, 143, pp. 179–188.

Heath, J.P., Harding, J.H., Sinclair, D.C. and Dean, J.S. (2019) 'The analysis of impedance spectra for core–shell microstructures: why a multiformalism approach is essential', *Advanced Functional Materials*, 29(38), #1904036.

Hewlett, P.C. and Liska, M. (2019) *Lea's Chemistry of Cement and Concrete*. 5th ed. United Kingdom: Elsevier.

Höhne, G.W.H., Hemminger, W.F. and Flammersheim, H.-J. (2003) *Differential Scanning Calorimetry*. 2nd ed. Laupheim: Springer.

Hsieh, G., Mason, T.O. and Pederson, L.R. (1996) 'Experimental limitations in impedance spectroscopy: Part II - electrode artifacts in three-point measurements on Pt/YSZ', *Solid State Ionics*, pp. 203–212.

Hu, J., Ge, Z. and Wang, K. (2013) 'Influence of cement fineness and water-to-cement ratio on mortar early-age heat of hydration and set times', *Construction and Building Materials*, 50, pp. 657–663.

Hu, X., Shi, C., Liu, X., Zhang, J. and de Schutter, G. (2019) 'A review on microstructural characterization of cement-based materials by AC impedance spectroscopy', *Cement and Concrete Composites*, 100, pp. 1–14.

Jen, G., Skalamprinos, S., Whittaker, M., Galan, I., Imbabi, M.S. and Glasser, F.P. (2017) 'The impact of intrinsic anhydrite in an experimental calcium sulfoaluminate cement from a novel, carbon-minimized production process', *Materials and Structures*, 50(2), #144. doi:10.1617/s11527-017-1012-z.

Kumar, A., Oey, T., Falzone, G., Huang, J., Bauchy, M., Balonis, M., Neithalath, N., Bullard, J. and Sant, G. (2017) 'The filler effect: The influence of filler content and type on the hydration rate of tricalcium silicate', *Journal of the American Ceramic Society*, 100(7), pp. 3316–3328. doi:10.1111/jace.14859.

Kwon, S.J., Feng, M.Q. and Park, S.S. (2010) 'Characterization of electromagnetic properties for durability performance and saturation in hardened cement mortar', *NDT and E International*, 43(2), pp. 86–95.

Langan, B.W., Weng, K. and Ward, M.A. (2002) 'Effect of silica fume and fly ash on

heat of hydration of Portland cement', *Cement and Concrete Research*, 32(7), pp. 1045–1051.

Li, Q. and Coleman, N.J. (2014) 'Hydration kinetics, ion-release and antimicrobial properties of white Portland cement blended with zirconium oxide nanoparticles', *Dental Material Journal*, 33(6), pp. 805–810. doi:10.4012/dmj.2014-174.

Liao, Y. and Wei, X. (2014) 'Penetration resistance and electrical resistivity of cement paste with superplasticizer', *Materials and Structures*, 47(4), pp. 563–570. doi:10.1617/s11527-013-0079-4.

Lothenbach, B., Winnefeld, F., Alder, C., Wieland, E. and Lunk, P. (2007) 'Effect of temperature on the pore solution, microstructure and hydration products of Portland cement pastes', *Cement and Concrete Research*, 37(4), pp. 483–491.

Lothenbach, B., Scrivener, K. and Hooton, R.D. (2011) 'Supplementary cementitious materials', *Cement and Concrete Research*, 41(12), pp. 1244–1256. doi:10.1016/j.cemconres.2010.12.001.

Lura, P., Friedemann, K., Stallmach, F., Mönnig, S., Wyrzykowsi, M. and Esteves, L.P. (2012) 'Kinetics of water migration in cement-based systems containing superabsorbent polymers', in *Application of Super Absorbent Polymers (SAP) in Concrete Constructions: State of the Art Report Prepared by Technical Committee 225-SAP*. RILEM/Springer, pp. 21–37.

Manchiryal, R.K. and Neithalath, N. (2008) 'Electrical property-based sensing of concrete: Influence of material parameters on dielectric response', *American Concrete Institute SP252*, pp. 23–40.

Marar, K. and Eren, Ö. (2011) 'Effect of cement content and water/cement ratio on fresh concrete properties without admixtures', *International Journal of the Physical Sciences*, 6(24), pp. 5752–5765. doi:10.5897/IJPS11.188.

Mason, T.O., Ford, S.J., Shane, J.D., Hwang, J.-H. and Edwards, D.D. (1998) 'Experimental limitations in impedance spectroscopy of cement-based materials', *Advances in Cement Research*, 10(4), pp. 143–150.

McCague, C., Bai, Y., Zhou, Q., and Basheer, P.A.M. (2014) 'Effect of calcium sulfates on the early hydration of calcium sulfoaluminate cement and the stability of embedded

aluminium', in *NUWCEM 2014. Second International Symposium on Cement-Based Materials for Nuclear Wastes (NUWCEM2014),* CEA, Avignon, France, 12 pp.

McCarter, W.J. (1994) 'A parametric study of the impedance characteristics of cement-aggregate systems during early hydration.', *Cement and Concrete Research*, 24(6), pp. 1097–1110.

McCarter, W.J. and Garvin, S. (1989) 'Dependence of electrical impedance of cement-based materials on their moisture condition', *Journal of Physics D: Applied Physics*, 22(11), pp. 1773–1776. doi:10.1088/0022-3727/22/11/033.

Mehta, P.K. and Monteiro, P.J.M. (2006) *Concrete: Microstructure, Properties, and Materials*. 3rd ed. California: McGraw-Hill.

Metrohm Autolab B.V, (2011) 'Electrochemical cell setup', *Autolab application note EC08*, pp. 1–3.

National Institute of Standards and Technology (2004) 'Primary standards and standard reference materials for electrolytic conductivity', NIST Special Publication 260-142, editors R.H. Shreiner and K.W. Pratt. 26 pp.

Navi, P. and Pignat, C. (1996) 'Simulation of cement hydration and the connectivity of the capillary pore space', *Advanced Cement Based Materials*, 4(2), pp. 58–67. doi:10.1016/S1065-7355(96)90052-8.

Neithalath, N. and Jain, J. (2010) 'Applications of electrical impedance methods in linking the structure of micro- and macro-porous concretes to their transport properties', *ACI Special Publication SP270*, pp. 33–50.

Novotný, R., Bartoníčková, E., Švec, J. and Mončeková, M. (2016) 'Influence of active alumina on the hydration process of Portland cement', *Procedia Engineering,* 151, pp. 80–86.

Orazem, M.E. and Tribollet, B. (2008) *Electrochemical impedance spectroscopy, Analysis*. Hoboken: Wiley.

Owsiak, Z. (2004) 'Dependence between the composition of pore solution and the expansion of mortar containing reactive aggregate', *Ceramics - Silikáty*, 49(2), pp. 109–114.

P. Gu, P. Xie and J. J. Beaudoin (1995) 'Some applications of AC impedance

spectroscopy in cement research', *Cement, Concrete, and Aggregates*, 17(2), pp. 113–118.

Pang, X., Bentz, D.P., Meyer, C., Funkhouser, G.P. and Darbe, R. (2013) 'A comparison study of Portland cement hydration kinetics as measured by chemical shrinkage and isothermal calorimetry', *Cement and Concrete Composites*, 39, pp. 23–32.

Pelletier-Chaignat, L, Winnefeld, F., Lothenbach, B., Le Saout, G., Müller, C.J. and Famy, C. (2011) 'Influence of the calcium sulphate source on the hydration mechanism of Portland cement-calcium sulphoaluminate clinker-calcium sulphate binders', *Cement and Concrete Composites*, 33(5), pp. 551–561.

Provis, J.L., Walls, P.A. and van Deventer, J.S.J. (2008) 'Geopolymerisation kinetics. 3. Effects of Cs and Sr salts', *Chemical Engineering Science*, 63(4480–4489).

Quennoz, A. (2011) *Hydration of C_3A with calcium sulfate alone and in the presence of calcium silicate*. PhD thesis, École polytechnique fédérale de Lausanne.

Raikova, G., Carpanese, P., Stoynov, Z., Vladikova, D., Viviani, M. and Barbucci, A.. (2009) 'Inductance correction in impedance studies of solid oxide fuel cells', *Bulgarian Chemical Communications*, 41(2), pp. 199–206.

Ramachandran, V.S. (1995) *Concrete Admixtures Handbook. Properties, Science, and technology*. 2nd edn. Ottawa, Ontario, Canada.: Noyes Publications.

Renaudin, G., Mesbah, A., Dilnesa, B.Z., Francois, M. and Lothenbach, B. (2015) 'Crystal chemistry of iron containing cementitious AFm layered hydrates', *Current Inorganic Chemistry*, 2, pp. 1–10. doi:10.2174/1877944105666150420235831.

Richardson, I.G., Girão, A.V., Taylor, R. and Jia, S.(2016) 'Hydration of water- and alkali-activated white Portland cement pastes and blends with low-calcium pulverized fuel ash', *Cement and Concrete Research*, 83, pp. 1–18.

Romano, R.C.O., Cincotto, M.A. and Pileggi, R.G. (2018) 'Hardening phenomenon of Portland cement suspensions monitored by Vicat test, isothermal calorimetry and oscillatory rheometry', *IBRACON*, 11(5), pp. 949–959.

Rosemount Analytical (2010) 'Conductance data for commonly used chemicals', 44, pp. 1–33.

Rothstein, D., Thomas, J.J., Christensen. B.J., and Jennings, H.M. (2002) ‘Solubility behavior of Ca-, S-, Al-, and Si-bearing solid phases in Portland cement pore solutions as a function of hydration time’, *Cement and Concrete Research*, 32(10), pp. 1663–1671. doi:10.1016/S0008-8846(02)00855-4.

Sáez del Bosque, I.F., Martínez-Ramírez, S. and Blanco-Varela, M.T. (2015) ‘Calorimetric study of white Portland cement hydration. Effect of nanosilica and temperature’, in *Proceedings of the 14th International Congress on the Chemistry of Cement*. Beijing, China.

Sanjuán, M.Á., Estévez, E. and Argiz, C. (2019) ‘Alkali ion concentration estimations in cement paste pore solutions’, *Applied Sciences*, 9(5), p. 992.

Scrivener, K.L., Snellings, R. and Lothenbach, B. (2017) *A practical guide to microstructural analysis of cementitious materials*. Boca Raton, Florida: CRC Press.

Scrivener, K.L., Juilland, P. and Monteiro, P.J.M. (2015) ‘Advances in understanding hydration of Portland cement’, *Cement and Concrete Research*, 78, pp. 38–56.

Scuderi, C.A., Mason, T.O. and Jennings, H.M. (1991) ‘Impedance spectra of hydrating cement pastes’, *Journal of Materials Science*, 26(2), pp. 349–353. doi:10.1007/BF00576526.

Sedaghat, A. (2016) *Cement heat of hydration and thermal control*. PhD thesis, University of South Florida.

Soboleva, T., Xie, Z., Shi, Z., Tsang, E., Navessin, T. and Holdcroft, S. (2008) ‘Investigation of the through-plane impedance technique for evaluation of anisotropy of proton conducting polymer membranes’, *Journal of Electroanalytical Chemistry*, 622(2), pp. 145–152.

Sosa Gallardo, A.F. and Provis, J.L. (2020) ‘Electrochemical ell design and characterisation of cement hydration by impedance spectroscopy’, *Journal of Materials Science*, 56, pp. 1203–1220.

Spragg, R., Villani, C., Snyder, K., Bentz, D., Bullard, J.W. and Weiss, J. (2013) ‘Factors that influence electrical resistivity measurements in cementitious systems’, *Transportation Research Record*, 2342(1), pp. 90-98.

Stefanou, G.D. and Larsinos, C. (1981) ‘Influence of mixing water on the setting time of

concrete', *International Journal of Cement Composites and Lightweight Concrete*, 3, pp. 45–48. doi:10.1016/0262-5075(81)90022-1.

Suresh, S. and Revathi, J. (2016) 'Effect of M-sand on setting time of high performance concrete', *Asian Journal of Research in Social Sciences and Humanities*, 6(10), p. 1648. doi:10.5958/2249-7315.2016.01118.7.

Tang, S.W., Cai, X.H., He, Z., Zhou, W., Shao, H.Y., Li, Z.J., Wu, T. and Chen. E. (2017) 'The review of early hydration of cement-based materials by electrical methods', *Construction and Building Materials*, 146, pp. 15–29.

Taylor, H.F.W. (1997) *Cement Chemistry*. 2nd edn, *Academic Press*. 2nd edn. London: Thomas Telford.

Topič, J. and Prošek, Z. (2017) 'Hydration process and mechanical properties of cement paste with recycled concrete powder and silica sand powder', *Acta Polytechnica CTU Proceedings*, 13, pp. 125–129. doi:10.14311/APP.2017.13.0125.

Tumidajski, P.J. (1996) 'Electrical conductivity of Portland cement mortars', *Cement and Concrete Research*, 26(4), pp. 529–534.

Tydlitát, V. and Tesárek, P. (2008) 'Effects of the type of calorimeter and the use of plasticers and hydrophobizers on the measured hydration heat development of gypsum', *Journal of Thermal Analysis and Calorimetry*, 91, pp. 791–796.

Vollpracht, A., Lothenbach, B., Snellings, R., and Haufe, J. (2015) 'The pore solution of blended cements: a review', *Materials and Structures*, 49(8), pp. 3341–3367. doi:10.1617/s11527-015-0724-1.

Wadsö, L., Cooper-Jensen, C.P. and Bentley, P.M. (2017) 'Assessing hydration disturbances from concrete aggregates with radiation shielding properties by isothermal calorimetry', *Physical Review Accelerators and Beams*, 20(4), pp. 1–8.

Wei, X., Xiao, L. and Li, Z. (2012) 'Prediction of standard compressive strength of cement by the electrical resistivity measurement', *Construction and Building Materials*, 31, pp. 341–346. doi:10.1016/j.conbuildmat.2011.12.111.

Whittington, H.W., McCarter, W.J. and Forde, M.C. (1981) 'The conduction of electricity through concrete', *Proceedings of The Institution of Civil Engineers*, 33(114), pp. 48–60.

Wong, H.S. and Buenfeld, N.R. (2009) 'Determining the water-cement ratio, cement

content, water content and degree of hydration of hardened cement paste: Method development and validation on paste samples', *Cement and Concrete Research*, 39(10), pp. 957–965. doi:10.1016/j..2009.06.013.

Xiao, L. and Wei, X. (2011) 'Early age compressive strength of pastes by electrical resistivity method and maturity method', *Journal of Wuhan University of Technology, Materials Science Edition*, 26(5), pp. 983–989. doi:10.1007/s11595-011-0349-3.

Xiong, C., Jiang, L., Zhang, Y., Chu, H. and Jiang, P. (2016) 'Characterization of sulfate diffusion into cement paste by low frequency impedance spectroscopy', *Materials Letters*, 174, pp. 234–237.

Xiong, X. and van Breugel, K. (2001) 'Isothermal calorimetry study of blended cements and its application in numerical simulations', *HERON*, 46(3), pp. 150–159.

Xu, L., Wang, P. and Zhang, G. (2012) 'Calorimetric study on the influence of calcium sulfate on the hydration of Portland cement–calcium aluminate cement mixtures', *Journal of Thermal Analysis and Calorimetry*, 110, pp. 725–731. doi:10.1007/s10973-011-1920-z.

Xu, Q., Hu, J., Ruiz, J.M., Wang, K. and Ge, Z. (2010) 'Isothermal calorimetry tests and modeling of cement hydration parameters', *Thermochimica Acta*, 499(1–2), pp. 91–99. doi:10.1016/j.tca.2009.11.007.

Xu, Z., Gu, P., Xie, P. and Beaudoin, J.J. (1993) 'Application of A.C. impedance techniques in studies of porous cementitious materials (III): ACIS behaviour of very low porosity cementitious systems', *Cement and Concrete Research*, 23, pp. 1007–1015.

Ylmén, R., Jäglid, U., Steenari, B.-M. and Panas, I. (2009) 'Early hydration and setting of Portland cement monitored by IR, SEM and Vicat techniques', *Cement and Concrete Research*, 39(5), pp. 433–439.

Ylmén, R., Wadsö, L. and Panas, I. (2010) 'Insights into early hydration of Portland limestone cement from infrared spectroscopy and isothermal calorimetry', *Cement and Concrete Research*, 40(10), pp. 1541–1546.

Ylmén, R. (2013) *Early hydration of Portland cement - An infrared spectroscopy perspective complemented by calorimetry and scanning electron microscopy*. PhD thesis, Chalmers University of Technology.

Yuan, X.-Z., Song, C., Wang, H. and Zhang, J. (2010) *Electrochemical impedance spectroscopy in PEM fuel cells*. London: Springer.

Zeghichi, L., Benghazi, Z. and Baali, L. (2014) 'The effect of the kind of sands and additions on the mechanical behaviour of S.C.C', *Physics Procedia*, 55, pp. 485–492. doi:10.1016/j.phpro.2014.07.070.

Zhang, Y.M. and Napier-Munn, T.J. (1995) 'Effect of particle size distribution, surface area and chemical composition on Portland cement strength', *Powder Technology*, 83, pp. 245–252.

Zhutovsky, S. and Kovler, K. (2009) 'Effect of water to cement ratio and degree of hydration on chemical shrinkage of cement pastes', *ConcreteLife'09: Concrete Durability and Service Life Planning*, RILEM, Haifa, Israel, pp. 47–54.